High-resolution infrared spectroscopy of isotopic impurity $Q_1(0)$ transitions in solid parahydrogen

David P. Weliky,[a] Karen E. Kerr, Teresa J. Byers, Yu Zhang, Takamasa Momose,[b] and Takeshi Oka

Department of Chemistry and Department of Astronomy and Astrophysics, The University of Chicago, Chicago, Illinois 60637

(Received 2 February 1996; accepted 5 June 1996)

We have made a high-resolution infrared spectroscopic study of the $Q_1(0)$ ($v=1\leftarrow 0$, $J=0\leftarrow 0$) vibrational transitions of the isotopic impurities D_2 and HD in solid parahydrogen. Each impurity has a spectrum composed of ~100 sharp lines spread over ~0.4 cm^{-1}. The linewidths vary, but are on the order of 10 MHz. These spectra make clear: (1) the infrared $Q_1(0)$ transitions of $J=0$ isotopic impurities are induced by the quadrupolar fields of nearby impurity $J=1$ molecules; and (2) the spectral pattern of strong $Q_1(0)$ lines is due to the splitting of the M-orientational levels of $J=1/J=0$ o-D_2 or $J=1/J=0$ HD nearest-neighbor (nn) impurity pairs. With the aid of several theoretical works, the strong lines in the D_2 and HD spectra can be individually and unambiguously assigned as specific quantum state $Q_1(0)$ transitions of nn impurity pairs containing p-D_2/o-D_2 or o-H_2/o-D_2, and o-H_2/HD, respectively. The assigned transitions of nn impurity pairs containing o-H_2 are confirmed by combination differences which agree to within 5×10^{-4} cm^{-1}, the instrumental precision. These assignments yield complete $Q_1(0)$ energy level diagrams for the nn impurity pairs o-H_2/o-D_2 and o-H_2/HD embedded in solid parahydrogen. The experimental energy level splittings are fit to a two parameter model which describes anisotropic interactions in the parahydrogen crystal. These experimental parameters appear to have significant contributions from the changes in renormalization and lattice constant around the heavier isotopic impurity. We have also assigned a few of the weaker spectral features as $Q_1(0)$ transitions of more distant impurity pairs, but the bulk of these transitions are yet to be assigned. They do form a distinctive pattern and are thought to be the $Q_1(0)$ transitions of impurity triples and larger clusters. This study is one of the few cases for which high-resolution laser spectroscopy has been successfully applied to the condensed phase and for which many of the transitions have rigorous quantum state assignments. [S0021-9606(96)03134-0]

I. INTRODUCTION

High-resolution spectroscopy has rarely been applied to solids because the lines are usually greatly broadened by homogeneous and inhomogeneous mechanisms.[1] A marked exception to this generalization is the parahydrogen (p-H_2) crystal, a hydrogen solid in which nearly all the molecules are in the $J=0$ rotational state. In solid hydrogen, the anisotropic intermolecular interactions are much smaller than the rotational energy level spacings, and J is retained as a good quantum number for individual molecules in the sample. The nearly isotropic interactions of the $J=0$ molecules in solid parahydrogen greatly decreases the usual solid state inhomogeneous broadening. The large energy mismatch between many spectral transitions and the phonon energies ($\nu_{\text{Debye}}\sim 70$ cm^{-1})[2] can also result in very small homogeneous broadening.

The first spectroscopic work on solid hydrogen was a 1955 infrared study on its fundamental vibrational band by Allin, Hare, and MacDonald.[3] Following the initial work, there were extensive solid hydrogen infrared and Raman studies done throughout the 1950's and 1960's.[4] The theory of solid hydrogen was also developed during this time, with Van Kranendonk and his coworkers as the principal architects. They explained most of the features of the observed spectra including the transition frequencies, linewidths, and intensities. Much of this theory has been summarized in a book by Van Kranendonk.[5]

The first high-resolution observation of solid parahydrogen was made in a series of pioneering microwave spectroscopy experiments by Hardy, Berlinsky, Harris, and their co-workers.[6–11] Transitions as sharp as 1 MHz half-width at half-maximum (HWHM) were observed. More recently, high-resolution infrared and stimulated Raman gain spectroscopy have been applied to solid parahydrogen and yielded linewidths as sharp as 7 MHz HWHM.[12,13] To date, the $Q_v(0)$ ($v=1,2,3$),[13–18] $Q_0(1)$,[6–11] $Q_1(1)$,[14,16,19] $S_0(0)$,[20] $U_0(0)$,[21] $U_1(0)$,[16] $U_1(1)$,[16] $W_0(0)$,[21,22] $W_1(0)$,[12,16,23,24] $W_1(1)$,[25] and $Y_0(0)$[25] transitions have been studied with high resolution. Additionally, sharp Stark field induced $Q_v(0)$ transitions have been observed.[13,26]

This paper focuses on the fundamental $Q_1(0)$ ($v=1\leftarrow 0$, $J=0\leftarrow 0$) vibrational transitions of the isotopic impurities D_2 and HD in solid parahydrogen. To date, there has been little spectroscopic work on isotopic impurities in

[a]Present address: Laboratory of Chemical Physics, NIDDK, NIH, Bethesda, MD 20892-0580.

[b]Present address: Department of Chemistry, Kyoto University, Kyoto, Japan.

solid parahydrogen. An initial infrared spectroscopic study by Chan *et al.*[27] of impurity D_2 yielded a $Q_1(0)$ vibrational spectrum of ten sharp ($\sim$10 MHz HWHM) lines whose assignment was mysterious. In the related system of impurity H_2 in solid HD, McKellar and Clouter[28] noted the sharpness of the impurity vibrational transitions. Additionally, the vibrational spectra of the chemical impurities CH_4[29,30] and CO[31] have been studied and relatively sharp ($\sim$300 MHz HWHM) lines were observed.

In contrast to isotopic and chemical impurities, $J=1$ orthohydrogen (o-H_2) ''rotational impurities'' have been extensively studied in solid parahydrogen.[2,5,14,16,19,32,33] The nearly free rotation of individual hydrogen molecules in the solid allows the retention of the rotational quantum number J and at low $J=1$ concentrations, the conversion of H_2 (or D_2) molecules from the $J=1$ to the $J=0$ state is extremely slow.[5] In most senses, o-H_2 and p-H_2 can be treated as separate molecular species. The o-H_2 impurity $Q_1(1)$ ($v=1\leftarrow 0$, $J=1\leftarrow 1$) vibrational transition sharpens as the o-H_2 concentration is reduced and at 0.2% [o-H_2], the measured amplitude modulated linewidth is $\sim$200 MHz HWHM.[34] Additionally, impurity pairs of o-H_2 molecules have sharp microwave[6–11] and infrared[14] spectra with microwave linewidths as narrow as 1 MHz HWHM.

HD and D_2 are ideal impurities without many of the complications of other chemical, rotational, or vibrational impurities. Unlike other chemical impurities, they are easily introduced into the parahydrogen lattice and do not cluster. Unlike $J=1$ o-H_2, their vibrational frequencies are hundreds of wave numbers from that of parahydrogen and the vibrational coupling between D_2 or HD and the host parahydrogen lattice is negligible. The average inter-impurity vibrational coupling is proportional to the impurity concentration and is reduced to $\sim$10 MHz at impurity concentrations of a few tenths percent, as we discuss in a forthcoming paper.[35] This is in marked contrast to the vibrational excitation of the parahydrogen lattice itself, in which the vibrational coupling manifests itself as a vibrational band of width $\sim 4\ \mathrm{cm}^{-1}$.[36]

Isotopic impurities have also been studied through their effects on other transitions. The o-H_2 impurity pair microwave spectra show spectral shifts and broadening with increasing D_2 concentration.[7] In other work, HD impurity has been shown to broaden the $S_0(0)$ ($v=0\leftarrow 0$, $J=2\leftarrow 0$) Raman transitions in solid parahydrogen.[37] In addition to spectroscopy, impurities have been studied through their effects on the heat capacity of solid parahydrogen.[38] The theoretical calculations which model these effects[39] are relevant to this paper.

The $Q_1(0)$ transition is the subject of this paper. For a single $J=0$ molecule or a group of $J=0$ molecules, the direct infrared $Q_1(0)$ transition is forbidden because of the lack of averaged multipole moments in the $J=0$ state. This transition is only allowed when some external electric field $\mathbf{E}$ interacts with the isotropic vibrational transition polarizability α_{01} and induces a dipole moment $\mu=\alpha_{01}\mathbf{E}$ in the $J=0$ molecule. $Q_1(0)$ observation is possible with a variety of electric fields including a radiation field (Raman effect)[33,40] or external Stark field (Condon effect).[26,41] Experimentally, solid parahydrogen also exhibits a strong $Q_1(0)$ transition in its direct infrared spectrum, as was first observed by Allin, Hare, and MacDonald.[3] In classic work by Gush *et al.*[32] the experimental variation of the p-H_2 $Q_1(0)$ infrared intensity with the $J=1$ o-H_2 concentration revealed that impurity o-H_2 molecules provide the electric field needed to induce the $Q_1(0)$ transition dipole. With the well-known parahydrogen lattice parameters and the expression for the quadrupolar field of an o-H_2 impurity, Sears and Van Kranendonk derived theoretical values for the integrated $Q_1(0)$ intensity which agreed quantitatively with experiment.[36] These experimental and theoretical works demonstrate the $J=1/J=0$ two molecule nature of the $Q_1(0)$ direct infrared transition, a topic which will be explored at length in this paper.

To date, one major difference between high-resolution solid parahydrogen spectroscopy and high-resolution gas phase spectroscopy is the certainty of the spectral assignment and precision of spectral fitting. In the gas phase, one typically has unambiguous state-specific assignment of each transition, as well as physically reasonable models whose parameters fit the transition frequencies and intensities to the experimental precision. By contrast, unambiguous assignment has only been achieved for some of the high-resolution solid parahydrogen spectra, the microwave[6–9] $Q_0(1)$ and infrared[19] $Q_1(1)$ o-H_2 pair transitions, the infrared $Q_3(0)$[17] spectra, and the $W_0(0)$[21] and $W_1(0)$[23,24] crystal field splittings. For most other spectra, only a few groups of strong lines are given some general assignments.

Additionally, some of the fully assigned spectra have not yet been fit to models whose parameters match the transition frequencies and intensities to the experimental precision. This is partly due to the large number of intermolecular interactions which contribute to the energy level patterns and partly because these interactions must be averaged over the large zero-point lattice motions of the molecules in the solid. This averaging, known as *renormalization*, is complicated because solid parahydrogen is a quantum crystal.[42] In quantum crystals, lattice dynamics cannot be treated by classical harmonic theory because the zero-point molecular motion is too large a fraction of the nearest-neighbor intermolecular separation. Renormalization of intermolecular interactions is not yet quantitatively understood in solid parahydrogen.

One of the achievements of the present work is that all of the strong infrared isotopic impurity $Q_1(0)$ transitions have been given rigorous quantum state assignments. In addition, most of these assigned transitions have been fit to a two parameter model. The values of these parameters can be understood in terms of the intermolecular interaction effects of impurity isotopic substitution, including the contributions from changes in lattice distances and renormalization. In particular, the experimental parameters appear to reflect the significant changes in renormalization due to the greater mass of the isotopic impurity. Hopefully, the present work will provide an experimental benchmark against which quantitative quantum crystal renormalization theories can be compared.

We clarify two semantic points. First, the $Q_1(0)$ transition in solid parahydrogen can be observed by a variety of

methods: direct infrared spectroscopy, Raman spectroscopy, and Stark field infrared spectroscopy. Unless otherwise stated, we are always referring to the direct infrared observation, even though we usually omit the words ''direct infrared''. Second, with the Pauli exclusion principle, the homonuclear hydrogenic isotopes can be divided into two types, J=even and J=odd, and there is negligible mixing or interconversion between these types in the absence of magnetic impurities. The J=even/odd states of H_2 (D_2) are labeled as para/ortho (ortho/para), in accord with the different spin statistics of $I=1/2$ (H) and $I=1$ (D) nuclei.

II. EXPERIMENT

A. Crystal preparation

In our experiments, hydrogen gas was first passed through a chemical purifier (Johnson–Matthey HP-50) and then converted to ~99.8% pure parahydrogen by passage through a column of APACHI nickel silica catalyst immersed in a liquid hydrogen bath. The resultant p-H_2 contained ~0.2% o-H_2 and ~0.04% HD residual impurities. The o-H_2 concentration could be reduced further to ~0.06% by pumping on the liquid hydrogen bath and lowering the conversion temperature. Prior to crystal growth, the p-H_2 gas was mixed in a ballast with a small amount of impurity isotope gas. The impurity gases were either normal-H_2 (n-H_2), normal-D_2 (n-D_2), ortho-D_2 (o-D_2), or HD. Unconverted n-H_2 contained p-H_2 and o-H_2 in the statistical ratio 1:3. Unconverted n-D_2 (Matheson CP grade) contained o-D_2 and p-D_2 in the statistical ratio 2:1. In some experiments, n-D_2 was converted at low temperature to ~97% o-D_2. HD (Cambridge) was 97% isotopically pure with ~1.5% each H_2 and D_2 impurities.

In the most recent experiments, we used an alternative conversion method to produce p-H_2 and o-D_2. The column of APACHI catalyst (converter) was pumped out and then immersed in a liquid helium bath. After waiting ~30 minutes for the APACHI catalyst to reach liquid helium temperature, H_2 or D_2 gas was flowed into the converter. The gas condensed on the catalyst and underwent conversion for ~45 min. The converter was then slowly raised out of the liquid helium bath and p-H_2 or o-D_2 gas was allowed to escape and flow into the ballast. The converter was designed such that the escaping vapor did not contact the catalyst and hence there was little back conversion to the normal species. This conversion method produced p-H_2 gas with ~0.2% o-H_2 impurity.

Transparent parahydrogen crystals were grown by vapor deposition at 7.25 K, as has been previously described.[12,13] Most crystals were grown in a cylindrical copper cell of length 11 cm and inner diameter 1.7 cm. The crystals grew radially inward from the cell walls and formed a hexagonal close-packed (hcp) structure with a radial c axis. Very transparent crystals were required for the observation of the sharpest spectral features. Poor transparency was usually the result of crystal cracking or significant chemical impurity concentrations in the sample. Cracking was a consequence of cooling too quickly from the 7.2 K growth temperature to the 4.2 K observation temperature. There was negligible heating of the sample from the color center laser radiation used in these experiments.

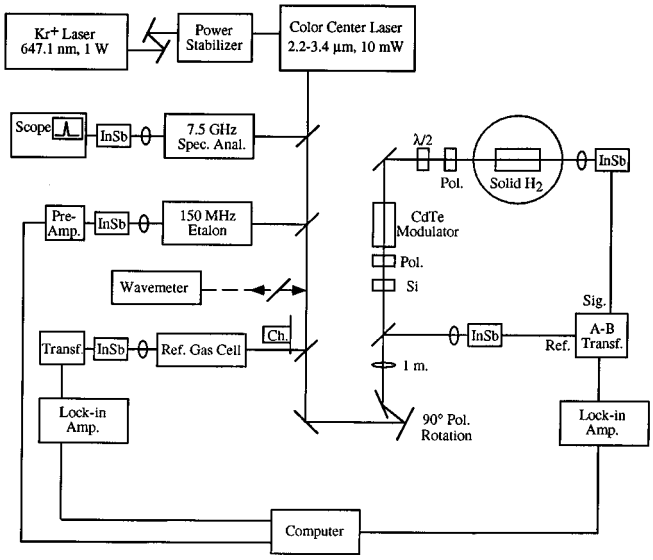

FIG. 1. Color center laser spectrometer. The color center laser was pumped by an amplitude-stabilized Kr^+ laser. Single mode operation of the color center laser was monitored by the 7.5 GHz spectrum analyzer while frequency calibration was made with the wavemeter, reference gas, and 150 MHz etalon. After the diagnostics and a 90° polarization rotation, a small portion of the beam was split off for common amplitude noise subtraction. The remaining radiation passed through a Si visible beam block, an infrared polarizer, and a CdTe electro-optic modulator. The polarization of the radiation was rotated by a half-wave plate, and then the beam went through another polarizer and the solid hydrogen sample before being focused onto an InSb detector. After noise subtraction by $A-B$ audio transformers, the signal was demodulated by a lock-in amplifier. Data acquisition and measurement of the experimental, reference gas, and 150 MHz etalon signals were made by a personal computer.

Our laser spectra showed that the concentration of any hydrogenic isotope in the crystal was approximately equal to its concentration in the gas mixture used to make the crystal. In addition, the $J=1$ impurity concentrations were determined from the FTIR integrated intensities of the crystalline $Q_1(1)$ $(v=1\leftarrow 0,\ J=1\leftarrow 1)$ transitions.[32,36] The estimated uncertainty in the impurity concentrations is ±10%, e.g., ±0.01% for a nominal impurity concentration of 0.1%.

For homonuclear H_2 and D_2, the rate of conversion between J=even and J=odd states is very slow. In the 4.2 K crystal, the J=even/J=odd ratio is approximately same as that in the room temperature converted gases. However, the J=even states come to thermal equilibrium with each other, as do the J=odd states, and at 4.2 K, $J=0$ ($J=1$) is the only even (odd) state with significant population. By contrast, there is rapid interconversion between all rotational states of heteronuclear HD and at 4.2 K, all HD molecules relax to the $J=0$ state.

B. Color center laser spectrometer

A schematic of the color center laser spectrometer used in these experiments is shown in Fig. 1. A commercial color center laser (Burleigh FCL-20) was pumped by ~1 W of the

647.1 nm line of a Kr^+ laser (Spectra-Physics 171-01). The Kr^+ power was amplitude stabilized with an acousto-optic modulator (Liconix 50SA). Several milliwatts of infrared radiation were generated by color center crystal #3 (F_A(II) RbCl:Li) at both the D_2 (2987 cm^{-1}) and the HD (3625 cm^{-1}) vibrational frequencies. A fraction of the laser power was directed through a spectrum analyzer and the detected output was observed on an oscilloscope to monitor the single mode quality of the laser. A wavemeter (Burleigh WA-20) was used to position the laser at the approximately correct frequency. More accurate frequency measurement was achieved by sending fractions of the laser power through a reference gas and through an etalon. The reference gas radiation was amplitude modulated and synchronously detected by a lock-in amplifier. The etalon (Burleigh CFT-500) was temperature-stabilized and had a free spectral range of 150 MHz. The combination of reference gas absorptions and etalon ticks gave a measurement reproducibility of ~15 MHz for the frequency spacing between transitions on the same scan.

After a 90° polarization rotation, the main beam passed through a Si visible beam block, an infrared polarizer, and a CdTe electro-optic modulator. The polarization of the radiation was rotated by a half-wave plate, and then the beam went through another polarizer and the solid hydrogen sample before being focused onto the InSb signal detector. A small portion of the infrared radiation was split off from the main beam and sent to a reference detector matched to the signal detector. The outputs of the signal and the reference detectors were subtracted from one another with $A-B$ transformers to reduce the common amplitude noise from the laser. This subtracted signal was demodulated by a lock-in amplifier. Data acquisition and measurement of the experimental, reference gas, and 150 MHz etalon signals were made by a personal computer.

Frequency scanning was achieved by ramping the voltage of the piezoelectric element on the laser end mirror. One percent of the ramp voltage was applied to the internal laser etalon through a variable gain amplifier. The amplifier gain was adjusted so that the end mirror and the laser etalon scanned smoothly together without mode hopping. Tracking the laser end mirror and etalon by this means achieved ~0.08 cm^{-1} continuous scans with ~3 MHz short-term frequency jitter.

C. Modulation and sensitivity

Two types of modulation were employed in these experiments: laser amplitude and laser frequency modulation. Amplitude modulation was effected by chopping the radiation at 1–2 kHz. The great advantage of amplitude modulation was that it gave undistorted line shapes and intensities. However, it was also the less sensitive modulation, giving a maximum sensitivity of $\Delta I/I \sim 1\times10^{-3}$.

Laser frequency modulation was a more sensitive technique and for most of the spectroscopy, tone-burst frequency modulation was employed. This was first developed for microwave frequencies[43] and has been more recently applied to the infrared.[44,45] Our tone-burst schematic is shown in Fig. 2. Synthesized radio frequency (rf) radiation (PTS 160) was coupled to a power amplifier (ENI 350L) and the amplifier output was sent to a CdTe electro-optic modulator. Frequency sidebands were generated by passing the color center laser radiation through the modulator. At rf modulation frequencies less than 50 MHz, a homemade wire inductor was put in series with the modulator and the modulation frequency was tuned to the LC resonance. By this means, infrared sidebands with at least 20% amplitude could be generated with less than 20 W of rf power. At higher frequencies, the inductor was not effective. With 50 W of rf power, sidebands of at least 10% amplitude could be generated at up to 120 MHz modulation depth.

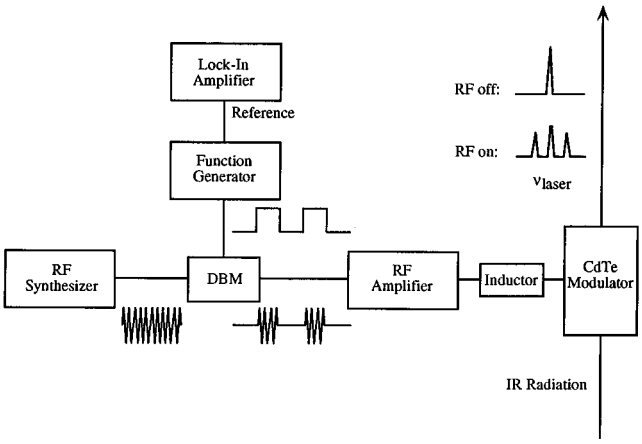

FIG. 2. Tone-burst frequency modulation. Synthesized rf (1–120 MHz) was chopped at 30 kHz and then amplified before being applied to a CdTe electro-optic modulator. After passing through the modulator, the color center laser radiation had amplitude-modulated frequency sidebands. This technique provided rf frequency modulation which could be conveniently detected at audio frequencies. Abbreviation: DBM, double balanced mixer.

With the tone-burst technique, the rf output (''tone'') was additionally 100% amplitude modulated (''burst'') at 30 kHz using a double balanced mixer (Mini-Circuits ZFM-3) and a function generator. This amplitude modulated the radiation sidebands and gave laser frequency modulation which could be detected in the kHz range, convenient for standard detectors and lock-in amplifiers. The sensitivity was limited by residual amplitude modulation or by etalons at the rf frequency, both of which were unwanted byproducts of the radiation passing through the CdTe crystal. Etaloning was reduced by tilting the modulator and all the optics in the spectrometer. Significant reduction in residual amplitude modulation was achieved by rotating the half-wave plate relative to the polarizer in the beam path. Careful rotation gave an order of magnitude increase in sensitivity while sacrificing ~30% of the signal power. Minimizing amplitude fluctuations of the Kr^+ pump laser was also crucial for attaining the greatest sensitivity. With the parameters of a 12 MHz tone, a 30 kHz burst, and a 300 ms detection time constant, a maximum sensitivity of $\Delta I/I \sim 5\times10^{-4}$ was achieved.

Tone-burst modulation and detection gave second derivative line shapes whose linewidths were a factor of 2–4 times sharper than the true linewidths. This reduction effectively increased our ability to resolve overlapping lines. However, in a spectrum with lines of varying widths, the broader transitions were often undermodulated. This gave spectra with distorted intensities, with the broader features suppressed relative to their sharper counterparts.

III. RESULTS

A. D_2 spectra

This work is predated by an initial spectroscopic study by Chan *et al.*[27] The previously observed D_2 impurity $Q_1(0)$ spectrum is shown in the top trace of Fig. 3 and contains ten tone-burst modulated lines whose linewidths are more than two orders of magnitude sharper than that of the p-H_2 lattice $Q_1(0)$ transition at 4153 cm^{-1}. The sharpness of the D_2 impurity lines shows how completely the impurity vibrational excitation is decoupled from the surrounding p-H_2 lattice. The assignment of the observed transitions was unknown and we did a series of experiments to gain additional information about this system.

In Chan *et al.* experiments, the p-H_2 crystal contained both $J=1$ o-H_2 and $J=1$ p-D_2 impurities. Both types of $J=1$ molecules should induce $Q_1(0)$ transitions in the neighboring impurity o-D_2 molecules but it was not known which $Q_1(0)$ transitions were induced by which type of $J=1$ molecule. New amplitude modulated spectra of the D_2 $Q_1(0)$ region are shown in the lower traces of Fig. 3. In the middle spectrum, the p-H_2 crystal contained both o-H_2 and p-D_2 and four clumps of transitions were observed. These transition groups are labeled (A–D) and correspond to the marked transitions in the tone-burst spectrum. In the lower spectrum, the crystal's p-D_2 concentration was greatly reduced and only two clumps of transitions remained. These experiments demonstrate that each kind of $J=1$ impurity induces two sets of D_2 $Q_1(0)$ transitions which are separated by $\sim$0.11 cm^{-1}. The p-D_2 induced transitions are displaced $\sim$0.03 cm^{-1} to lower frequency from their o-H_2 induced counterparts. As shown in the upper trace of Fig. 3, the o-H_2 induces a higher frequency quartet and a lower frequency singlet while the p-D_2 induces a higher frequency multiplet and a lower frequency doublet. This assignment is in agreement with the linewidth argument of Chan.[46]

Several different crystals were studied with varying o-H_2 and o-D_2 content. The individual integrated intensities of both the o-H_2 induced singlet and the o-H_2 induced quartet scaled approximately with the product $[o\text{-}H_2][o\text{-}D_2]$. Depending on the impurity concentrations, the spectral linewidths varied between approximately 2 and 150 MHz, and were generally sharper in crystals with lower impurity content. These linewidth variations are discussed in detail in other papers.[35,47]

After the first set of experiments, there was a great increase in spectrometer sensitivity due to the tone-burst modulation improvements discussed in Sec. II C. Because of this sensitivity increase, we were able to observe many new lines in the D_2 $Q_1(0)$ region. Some of these new tone-burst modulated spectra are shown in Fig. 4 and the frequencies of all of the assigned transitions are listed in Table I. There was a frequency shift of up to a few thousandths of a cm^{-1} when comparing the same transition in two different crystals. This shift was approximately the same for all transitions and is ascribed to a matrix shift difference between the two different crystals. Any given table lists the frequencies for a particular crystal with the listed impurity concentrations.

Several of the strongest new lines [Figs. 4(a) and 4(d)] were two times broader than the sharpest previously observed transitions [Figs. 3(A), 3(C), 4(b), and 4(e)]. Undermodulation was one reason for their absence in the previous tone-burst spectra. We used these linewidth differences to

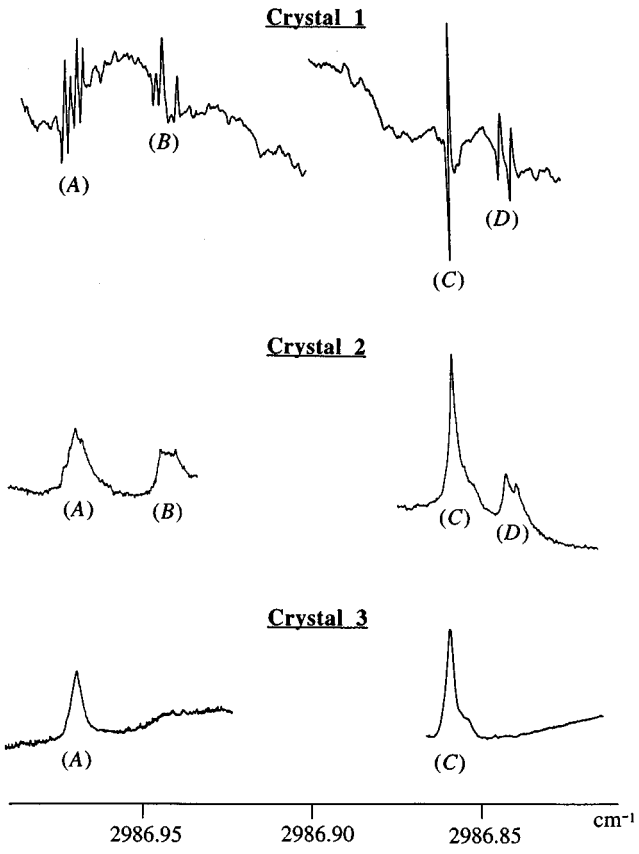

FIG. 3. Early observations of the impurity D_2 $Q_1(0)$ spectra in solid parahydrogen. Infrared spectra from three different parahydrogen crystals are presented. The top trace displays the tone-burst modulated spectrum of a crystal which was doped with n-D_2 and contained 0.4% o-D_2, 0.2% p-D_2, and 0.06% o-H_2 impurities.[27] Four clumps of transitions were observed and are marked (A–D) in order of descending frequency. The middle traces display amplitude modulated spectra of a second crystal which was also doped with n-D_2 and contained 0.4% o-D_2, 0.2% p-D_2, and 0.2% o-H_2 impurities. The transitions (A–D) were all observed but are less well resolved than in the tone-burst modulated spectra. The most intense feature (C) had a peak absorption of $\sim$20% and a width of $\sim$31 MHz HWHM. The bottom traces display amplitude modulated spectra of a third crystal which was doped with o-D_2 and contained 0.4% o-D_2, 0.01% p-D_2, and 0.2% o-H_2 impurities. In these scans, only the (A) and (C) transitions were observed. From all these spectra, we conclude that $J=1$ o-H_2 induces the two sets of o-D_2 $Q_1(0)$ transitions marked (A) and (C), and that $J=1$ p-D_2 induces the two sets of o-D_2 $Q_1(0)$ transitions marked (B) and (D).

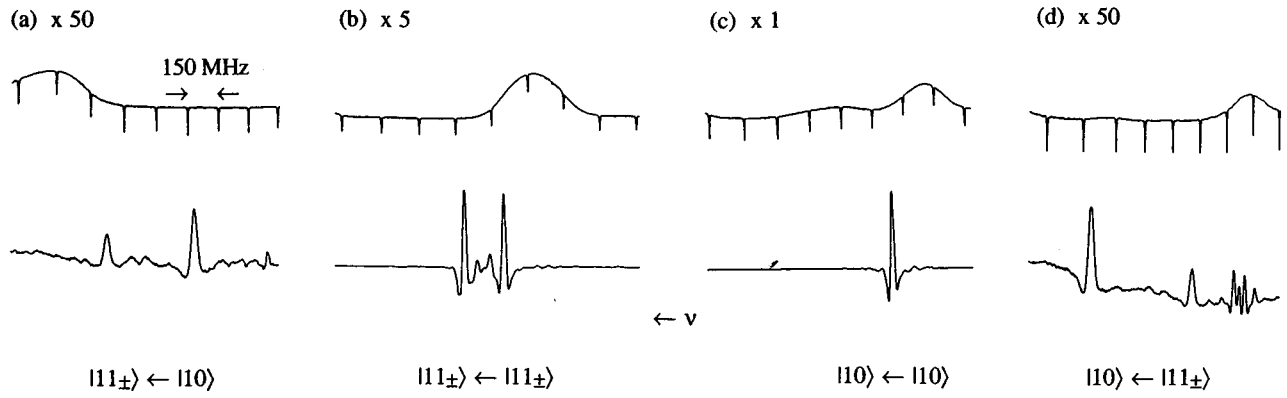

FIG. 4. More recent impurity D_2 $Q_1(0)$ spectra. The parahydrogen crystal contained 0.25% o-D_2, 0.2% o-H_2, and 0.01% p-D_2 impurities. Traces (a)–(d) are tone-burst modulated spectra spanning ~0.04 cm^{-1} regions about 2987.09, 2986.97, 2986.86, and 2986.73 cm^{-1}, respectively. The upper reference gas/etalon traces are also shown and contain amplitude modulated C_2H_4 absorptions at 2987.1068, 2986.9661, 2986.8536, and 2986.7185 cm^{-1}. The tone-burst modulated spectra were taken with 17 MHz sidebands and parallel laser polarization. They contain the most intense observed transitions which are assigned with the $|1M\rangle$ labels of the nearest-neighbor o-H_2/o-D_2 impurity pair, as described in Secs. IV and V of the text. The (b) and (c) features correspond to the (A) and (C) features of Fig. 3, respectively.

aid in spectral assignment, as discussed in Secs. IV and V.

Most of the observed transitions had a pronounced intensity dependence with laser polarization. Two examples are shown in Fig. 5, the o-H_2 induced quartet and the p-D_2 induced doublet. The direction of the laser polarization was

TABLE I. Assigned o-H_2 induced and p-D_2 induced $Q_1(0)$ transitions of D_2.

$J=1$ inducer	Frequency (cm^{-1})[a]	Pair Type[b]	Assignment[c]
o-H_2	2987.1004	nn oop	$\|11_+\rangle\leftarrow\|10\rangle$
o-H_2	2987.0967	nn oop	$\|11_-\rangle\leftarrow\|10\rangle$
o-H_2	2987.0945	nn ip	$\|11_+\rangle\leftarrow\|10\rangle$
o-H_2	2987.0869	nn ip	$\|11_-\rangle\leftarrow\|10\rangle$
o-H_2	2986.9757	nn oop	$\|11_-\rangle\leftarrow\|11_-\rangle$
o-H_2	2986.9739	nn ip	$\|11_-\rangle\leftarrow\|11_-\rangle$
o-H_2	2986.9722	nn ip	$\|11_+\rangle\leftarrow\|11_+\rangle$
o-H_2	2986.9703	nn oop	$\|11_+\rangle\leftarrow\|11_+\rangle$
o-H_2	2986.8592	nn ip,oop	$\|10\rangle\leftarrow\|10\rangle$
o-H_2	2986.7463	nn ip	$\|10\rangle\leftarrow\|11_-\rangle$
o-H_2	2986.7381	nn oop	$\|10\rangle\leftarrow\|11_-\rangle$
o-H_2	2986.7366	nn ip	$\|10\rangle\leftarrow\|11_+\rangle$
o-H_2	2986.7291	nn oop	$\|10\rangle\leftarrow\|11_+\rangle$
o-H_2	2986.9348	nnn	$\|10\rangle\leftarrow\|10\rangle$
p-D_2	2986.9475 2986.9427	nn oop	$\|11_\pm\rangle\leftarrow\|11_\pm\rangle$
p-D_2	2986.9462 2986.9415	nn ip	$\|11_\pm\rangle\leftarrow\|11_\pm\rangle$
p-D_2	2986.8439	nn ip	$\|10\rangle\leftarrow\|10\rangle$
p-D_2	2986.8405	nn oop	$\|10\rangle\leftarrow\|10\rangle$

[a]The o-H_2 induced transitions were measured with a parahydrogen crystal which contained approximately 0.2% o-H_2, 0.25% o-D_2, 0.01% p-D_2, and 0.04% HD impurities. The p-D_2 induced transitions were measured with a parahydrogen crystal which contained approximately 0.2% o-H_2, 0.4% o-D_2, 0.2% p-D_2, and 0.04% HD impurities.

[b]Abbreviations: nn—nearest-neighbor, nnn—next-nearest-neighbor, ip—in-plane, oop—out-of-plane.

[c]See Secs. III–V of the text.

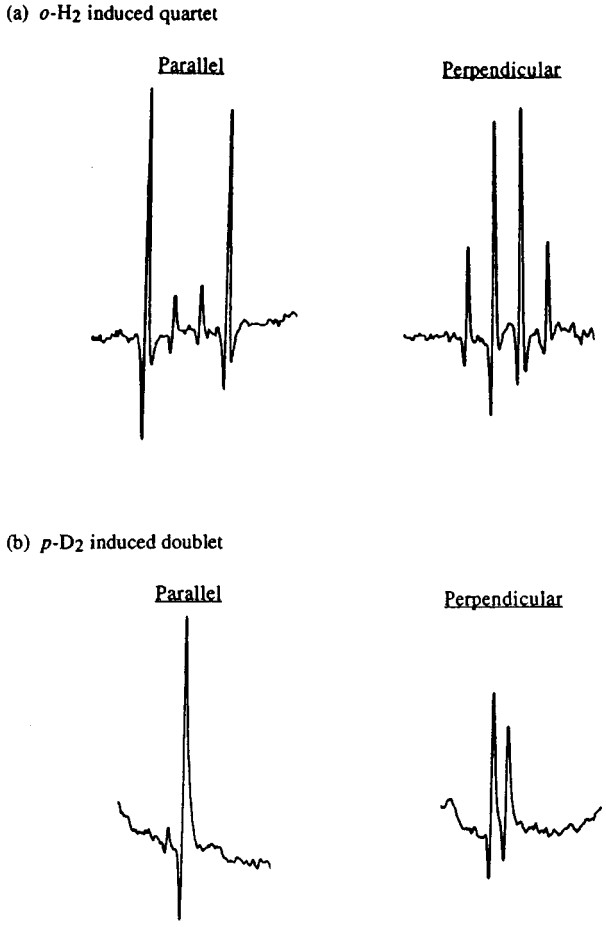

FIG. 5. Laser polarization dependence of the relative intensities of impurity D_2 $Q_1(0)$ transitions. Tone-burst modulated spectra in (a) and (b) are of the o-H_2 induced quartet and p-D_2 induced doublet, features (A) and (D) in Fig. 3, respectively. Frequency increases from right to left in all scans. The individual quartet transitions in (a) are separated by ~50 MHz and the individual doublet transitions in (b) are separated by ~100 MHz. The laser polarization was relative to the unique c axis of the crystal.

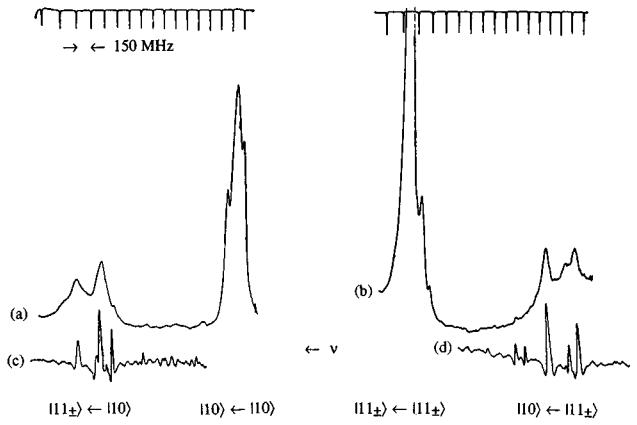

FIG. 6. Impurity HD $Q_1(0)$ infrared spectra in solid parahydrogen. The crystal contained 0.24% HD and 0.2% o-H_2 impurities and the laser polarization was parallel. Traces (a) and (b) are amplitude modulated spectra spanning ~0.08 cm^{-1} regions about 3624.74 and 3624.54 cm^{-1}, respectively. The transitions are assigned with $|1M\rangle$ labels of the o-H_2/HD impurity pair, as described in Secs. IV and V of the text. The peak absorptions of the $|11_{\pm}\rangle \leftarrow |10\rangle$ and $|10\rangle \leftarrow |11_{\pm}\rangle$ transitions are a few percent. Traces (c) and (d) are tone-burst modulated spectra of these transitions using 12 MHz sidebands.

relative to the crystalline c axis. This axis was unidirectional over the small cross section probed by the laser beam (~3 mm^2).

In addition to the strongest transitions listed in Table I, there were ~100 weaker lines in the D_2 $Q_1(0)$ spectra. More spectra are presented in Sec. V.

B. HD spectra

The HD impurity $Q_1(0)$ spectrum was first observed by Chan.[30] In a parahydrogen crystal containing ~1.5% HD and ~0.2% o-H_2 impurities, he observed two features in the tone-burst spectrum with frequencies 3624.7163 and 3624.5793 cm^{-1}. With greater sensitivity and much lower HD concentration, we were able to observe many more transitions, some of which are shown in Fig. 6. The HD spectra had many qualitative similarities with the D_2 spectra. At the crystal temperature of 4.2 K, all of the HD impurities were in the $J=0$ state, so most of the observed HD $Q_1(0)$ transitions would be induced by the residual $J=1$ o-H_2 impurities in the lattice. Table II lists the frequencies of the assigned HD transitions. We had only one reference line in the frequency region of most of the HD transitions. All HD frequencies were measured relative to this reference using an etalon spacing of 0.0050 cm^{-1}.

Similar to the D_2 $Q_1(0)$ spectra, the HD $Q_1(0)$ spectra contained ~100 other weaker lines, in addition to the strongest transitions displayed in Fig. 6 and listed in Table II. Complete D_2 and HD $Q_1(0)$ spectra and lists of frequencies are available upon request.

TABLE II. Assigned o-H_2 induced $Q_1(0)$ transitions of HD.

Frequency (cm^{-1})[a]	Pair type[b]	Assignment[c]
3624.7851	nn oop	$\|11_-\rangle \leftarrow \|10\rangle$
3624.7819	nn oop	$\|11_+\rangle \leftarrow \|10\rangle$
3624.7791	nn ip	$\|11_+\rangle \leftarrow \|10\rangle$
3624.7733	nn ip	$\|11_-\rangle \leftarrow \|10\rangle$
3624.7205	nn oop	$\|11_-\rangle \leftarrow \|11_-\rangle$
3624.7178	nn ip	$\|11_-\rangle \leftarrow \|11_-\rangle$
3624.7159	nn ip	$\|11_+\rangle \leftarrow \|11_+\rangle$
3624.7132	nn oop	$\|11_+\rangle \leftarrow \|11_+\rangle$
3624.5810	nn ip,oop	$\|10\rangle \leftarrow \|10\rangle$
3624.5258	nn ip	$\|10\rangle \leftarrow \|11_-\rangle$
3624.5181	nn ip	$\|10\rangle \leftarrow \|11_+\rangle$
3624.5166	nn oop	$\|10\rangle \leftarrow \|11_-\rangle$
3624.5124	nn oop	$\|10\rangle \leftarrow \|11_+\rangle$
3624.6891	nnn	$\|11_+\rangle \leftarrow \|10\rangle$
3624.6849	nnn	$\|11_-\rangle \leftarrow \|10\rangle$
3624.6802	nnn	$\|11_+\rangle \leftarrow \|11_+\rangle$
3624.6777	nnn	$\|11_-\rangle \leftarrow \|11_-\rangle$
3624.6695	nnn	$\|10\rangle \leftarrow \|10\rangle$
3624.6618	nnn	$\|10\rangle \leftarrow \|11_-\rangle$
3624.6607	nnn	$\|10\rangle \leftarrow \|11_+\rangle$

[a]These frequencies were measured with a parahydrogen crystal which contained approximately 0.2% o-H_2 and 0.24% HD impurities.
[b]Abbreviations: nn—nearest-neighbor, nnn—next-nearest-neighbor, ip—in-plane, oop—out-of-plane.
[c]See Secs. III–V of the text.

IV. $J=1/J=0$ IMPURITY PAIR MODEL

A. Qualitative picture

As discussed in Sec. I, the $Q_1(0)$ transition is infrared forbidden in an isolated $J=0$ molecule or a collection of $J=0$ molecules because of the lack of averaged multipole moments in the $J=0$ state. Experimentally, the solid p-H_2 lattice exhibits a strong infrared p-H_2 $Q_1(0)$ transition because of the presence of $J=1$ impurities in the solid. As formulated by Sears and Van Kranendonk,[36] the quadrupolar fields of the $J=1$ impurities induce the $Q_1(0)$ infrared transition in the neighboring p-H_2 molecules. The largest perturbation of the $Q_1(0)$ energy is the hopping of the vibrational excitation (vibron) between neighboring p-H_2 molecules. This gives a vibrational energy band of width ~4 cm^{-1} and results in a p-H_2 $Q_1(0)$ infrared linewidth of ~0.2 cm^{-1} HWHM.[16]

The $Q_1(0)$ vibrational spectrum of the impurities (cf. Figs. 3–6) is qualitatively different from that of the p-H_2 lattice molecules because the vibrational coupling is so much weaker between the more distant impurity molecules than between the p-H_2 lattice molecules. The vibron hopping scales approximately with the impurity concentration,[35] so for experimental impurity concentrations of a few tenths percent, the hopping interaction would be on the order of 10^{-3} cm^{-1}. The frequency separations of the strong impurity D_2

and HD infrared transitions were much more than 10^{-3} cm^{-1} and were likely due to interactions other than vibrational coupling.

Because of the R^{-4} dependence of quadrupolar fields, more than 90% of the p-H_2 $Q_1(0)$ transition intensity comes from p-H_2 molecules which are nearest-neighbors (nn) of a $J=1$ impurity.[36] As a starting point, we assumed that this would also be true for the D_2 and HD impurity $Q_1(0)$ transitions. At the impurity concentrations used in these experiments, only a small minority of the isotopic impurities were part of nn $J=1/J=0$ *impurity pairs* (e.g., nn o-H_2/o-D_2). The vast majority of isotopic impurities were ''isolated'', that is all 12 of their nn were p-H_2 molecules. With typical concentrations $[J=0$ isot. imp.$]=2\times10^{-3}$ and $[J=1]=2\times10^{-3}$, the statistical ratio [nn imp. pairs]/[isol. imp.]$\cong2.5\times10^{-2}$. The minority nn impurity pairs contribute most of the isotropic impurity $Q_1(0)$ infrared intensity, while the majority isolated impurities contribute little to the $Q_1(0)$ infrared intensity. However, these isolated impurities should make the major intensity contribution to the isotopic impurity Raman and Stark field induced $Q_1(0)$ spectra.[13] The Stark field induced spectrum has been observed for D_2 impurities in solid parahydrogen and most of the intensity was contained in a sharp line at 2986.9434 cm^{-1}.[13,48,49] This transition frequency did not correspond to any of the strong lines in the impurity D_2 $Q_1(0)$ direct infrared spectrum. The striking difference between the direct infrared and Stark field induced $Q_1(0)$ spectra gave credence to the idea that different types of isotopic impurities were being observed in the two different spectra.

In the direct infrared spectra, the strong signals should be comprised of a vibrational excitation of an impurity $J=0$ D_2 or HD and an accompanying orientational transition of the nn impurity $J=1$ molecule. This sort of model is appealing because the observed $Q_1(0)$ frequency splittings could be explained by the energy splittings of the M-orientational states of the $J=1$ molecule, while the observed polarization dependences could be explained by the orientational nature of the $J=1/J=0$ transition moment. In their calculations of the p-H_2 lattice $Q_1(0)$ transition, Sears and Van Kranendonk averaged over all of the orientational effects relating to the $J=1$ inducer molecules. This was appropriate because only a single relatively broad line had been observed. By contrast, our isotopic impurity $Q_1(0)$ spectra contain many sharp lines, so we need to consider $J=1/J=0$ impurity pair interactions in much greater detail.

We first give a qualitative picture of impurity energetics in a solid. Figure 7(a) shows the nondegenerate $Q_1(0)$ vibrational transition of a single gas phase o-D_2 molecule. D_2 is shown in both Figs. 7 and 8, but the same qualitative picture holds for HD. In Fig. 7(b), the isolated o-D_2 impurity is embedded in the parahydrogen solid, and both the ground and excited D_2 vibrational levels are shifted to lower energies by isotropic intermolecular interactions. Because of the unequal shifts of the $v=0$ and $v=1$ levels, the solid state vibrational frequency differs from that in the gas phase. The vibrational frequency *matrix shift* ($\nu_{\text{solid}}-\nu_{\text{gas}}$) is $\sim$6.63 and ~-7.42 cm^{-1} for the $Q_1(0)$ transitions of isolated impurity

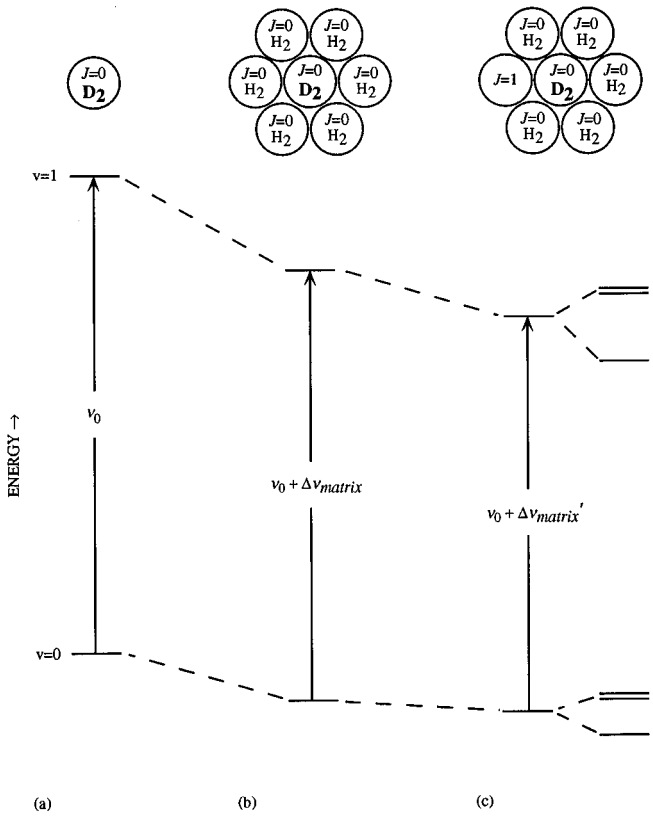

FIG. 7. D_2 $Q_1(0)$ energy level diagrams. In (a), the vibrational transition of a single gas phase $J=0$ o-D_2 molecule is displayed ($\nu_0=2993.57$ cm^{-1}) (Ref. 50). In (b), the ''isolated'' o-D_2 impurity is embedded in the parahydrogen solid, and both the ground and excited state vibrational levels are shifted to lower energies from their gas phase values. The inequality of these shifts results in a small vibrational frequency matrix shift, ~-6.63 cm^{-1} for D_2. In (c), replacement of a nearest-neighbor $J=0$ p-H_2 molecule by a $J=1$ impurity molecule further lowers the D_2 impurity energy levels and splits the three M-orientational levels of the impurity pair $J=1$ molecule. The additional matrix shift is ~-0.01 cm^{-1}.

D_2 and HD in solid parahydrogen, respectively.[13,48–50] If one assumes that the shifts in the $v=0$ and $v=1$ states are proportional to the isotropic impurity's isotropic polarizability (true for induction and dispersion interactions), then the experimental matrix shifts correspond to a solid state binding energy of $\sim$8 cm^{-1} for a $v=0$ p-H_2/$v=0$ o-D_2 or a $v=0$ p-H_2/$v=0$ HD pair. This value approximately agrees with earlier determinations of pair binding energies in solid hydrogen.[2] In Fig. 7(c), replacement of a $J=0$ p-H_2 by a $J=1$ molecule lowers the $v=0$ and $v=1$ energies by $\sim$0.2 cm^{-1},[5,24,51] with an additional impurity pair $Q_1(0)$ matrix shift of ~-0.01 cm^{-1}.

Furthermore, the three M-orientational levels of the impurity pair $J=1$ molecule are split for both the ground and excited o-D_2 vibrational states. These splittings arise from anisotropic $J=1/J=0$ intermolecular interactions, as shown in Fig. 8. In the limit of weak intermolecular interactions, the $J=1$ molecule will be in one of its three nearly degenerate $|1M\rangle$ orientational states. The simplest computational case is a single $J=1/J=0$ pair, as shown in Fig. 8(a). The orientational states are quantized along the intermolecular pair axis

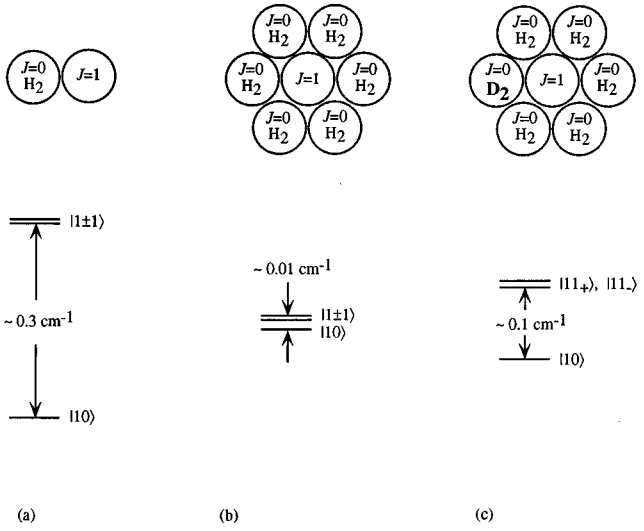

FIG. 8. Energy level diagrams of $J=1/J=0$ anisotropic interactions (Ref. 7). The $|1M\rangle$ orientational states and splittings are given for different molecular configurations. In (a), a single $J=1/J=0$ molecular pair is considered. The intermolecular axis is the quantization axis and the states are split by a few tenths of a wave number. In (b), a single $J=1$ impurity molecule is embedded in an hcp crystal of $J=0$ parahydrogen. The crystalline c axis is the quantization axis and the orientational splitting is reduced to less than 0.01 cm^{-1} (Ref. 18). In (c), an impurity pair is formed from replacement of one of the nearest-neighbor $J=0$ p-H_2 by an impurity $J=0$ o-D_2. The orientational states are quantized along the impurity pair intermolecular axis with a $|10\rangle/|11_{\pm}\rangle$ splitting of $\sim$0.1 cm^{-1}.

and are split into a lower energy $|10\rangle$ state and a higher energy degenerate pair of states $|1\pm1\rangle$. There have been numerous calculations of the energy splitting, most giving a value somewhere between 0.1 and 1 cm^{-1}.[7] The next simplest computational case is a single $J=1$ impurity in an otherwise perfect hexagonal close-packed (hcp) parahydrogen lattice. This is shown in Fig. 8(b) and is qualitatively different from an isolated pair. In Fig. 8(b), the $|1M\rangle$ states are quantized along the crystalline c axis and are only split by $\sim$0.01 cm^{-1}. Nakamura[52] first explained this splitting energy reduction using accidental cancellation of pairwise anisotropic $J=1/J=0$ interactions in an hcp lattice with a single nn intermolecular distance. Using nmr spectroscopy, the solid state $|10\rangle/|1\pm1\rangle$ splitting was determined to be $\sim5.8\times10^{-3}$ cm^{-1}.[53,54] A more recent measurement is 7.1×10^{-3} cm^{-1}, with the $|10\rangle$ state at lower energy than the $|1\pm1\rangle$ states.[18]

For our spectra, one of the surrounding neighboring $J=0$ p-H_2 molecules is replaced by a $J=0$ isotopic impurity, as shown in Figs. 7(c) and 8(c). The symmetry of the hcp lattice is broken and the accidental cancellation is disrupted. Calculations[24,39,51] show that the impurity pair states are quantized along the impurity pair intermolecular axis and that the energy splitting is much larger than in the pure p-H_2 crystal [cf. Fig. 8(b)]. Additionally, the formerly degenerate $|1\pm1\rangle$ states are split. The correct eigenstates are linear combinations of the $|1\pm1\rangle$ states, $|11_+\rangle$ and $|11_-\rangle$, where the ''+'' and ''−'' subscripts refer to the parity relative to the symmetry plane of the lattice.

B. Mathematical model

We now present a more mathematical description of $J=1/J=0$ impurity pair interactions in solid parahydrogen. These interactions were first considered by Kokshenev[39] and more recently by Byers and Oka.[24,51] We consider only pairwise interactions in an hcp crystal.

A pair of diatomic molecules has an intermolecular potential $A(\omega_1,\omega_2,R)$ which can be expanded in terms of Racah spherical harmonics $C_{lm}(\omega)$ as[5]

$$A(\omega_1,\omega_2,R) = \sum_{l_1 l_2 m_1 m_2} A_{l_1 l_2 m_1 m_2}(R) C_{l_1 m_1}(\omega_1) C_{l_2 m_2}(\omega_2), \tag{1}$$

where R is the length of the intermolecular vector $\mathbf{R}$ connecting the centers of masses of the two molecules, $\omega_1=(\theta_1,\phi_1)$ is the orientation of molecule 1's internuclear vector relative to $\mathbf{R}$, $\omega_2=(\theta_2,\phi_2)$ is the orientation of molecule 2's internuclear vector relative to $\mathbf{R}$, and the $A_{l_1 l_2 m_1 m_2}(R)$ are the scalar functions of R which represent the strengths of different angle-dependent interactions. These functions implicitly contain averaging over the intramolecular vibrational wave functions and hence will depend on the vibrational states of the two molecules. We consider restrictions on l_1, l_2, m_1, and m_2. Axial symmetry of the pair requires that $m_1=-m_2=m$.[5] We are concerned with $J=1/J=0$ pairs and only consider the spherical harmonics which have nonzero diagonal elements in the rotational subspaces of the molecules. The isotropic and anisotropic contributions to the $J=1/J=0$ pairwise interaction are represented by the $l_1=0$, $l_2=0$, and $l_1=2$, $l_2=0$ terms, respectively.

The isotropic term, $A_{00}(R)$, is nonzero for both $J=1/J=0$ and $J=0/J=0$ pairwise interactions and leads to the vibrational matrix shift shown in Figs. 7(b)–7(c). With consideration of zero-point motion, A_{00} can be calculated from the H_2/H_2 isotropic pair potential curve [cf. Fig. 9(a)]. At small intermolecular distances, the potential is dominated by repulsive valence terms which fall off exponentially with R, and at large separations, the potential is dominated by attractive dispersion terms which fall off as R^{-n}, $n\geqslant6$. At the average nn distance $R_0\sim3.783$ Å,[2] the valence and dispersion interactions both make large contributions to the isotropic potential and result in a static pair binding energy of $\sim$25 cm^{-1}.[5,55] Induction contributes $\sim$0.1 cm^{-1} to the nn $J=1/J=0$ pair binding energy[5] and is dominated by the quadrupole-induced dipole interaction. The second order EQQ interaction is calculated from quadrupole-induced rotational state mixing and also contributes $\sim$0.1 cm^{-1} to the binding energy.[24,51] Induction and second order EQQ fall off with pair distance as R^{-8} and R^{-10}, respectively.

Energy calculations on the $J=1$ p-$D_2/J=0$, $v=1$ o-D_2 impurity pair must also include the vibrational coupling between the two D_2 molecules. Although this vibrational hopping is not resonant, it does lead to a vibrational energy shift of $\sim+0.016$ cm^{-1} for this type of nn impurity pair.[46] For

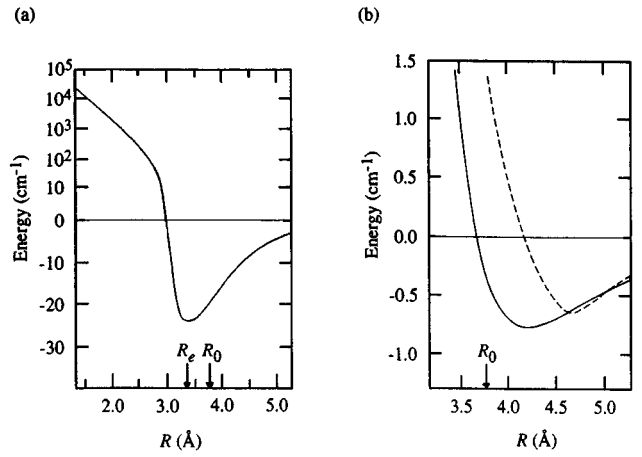

FIG. 9. H_2/H_2 pair potentials. In (a), one calculation of the total isotropic H_2/H_2 pair potential $A_{00}(R)$ is presented (Refs. 5 and 55). The abscissa is the pair intermolecular distance. The energy ordinate is linear below 7 cm^{-1} and logarithmic above 7 cm^{-1}. The distances R_e and R_0 are defined by the minimum in the isotropic potential and the average solid state nearest-neighbor intermolecular distance, respectively. In (b), we present two calculations of $B(R)$, which represents the strength of the $C_{20}(\omega)$ pairwise anisotropic interaction. The solid trace is from Ref. 5 and the dotted trace is from Ref. 56.

other kinds of nn impurity pairs, the hopping shift is less than 10^{-4} cm^{-1} because of the large vibrational frequency difference between the two molecules.

The anisotropic $J=1/J=0$ pair potential is represented by a single term from Eq. (1), $B(R)C_{20}(\omega)$, where ω refers to the orientation of the $J=1$ molecule relative to the pair axis and $C_{20}(\omega)=C_{20}(\theta,\phi)=1/2(3\cos^2\theta-1)$. Because of this term, the three $|1M\rangle$ states of the $J=1$ molecule are split into the eigenstates $|10\rangle$ and $|1\pm1\rangle$, with eigenvalues $2B(R)/5$ and $-B(R)/5$, respectively [cf. Fig. 8(a)]. The same types of interactions (dispersion, valence, induction, second order EQQ) which contribute to the isotropic potential $A_{00}(R)$ also have anisotropic components, creating a potential well for $B(R)$ of $\sim$0.7 cm^{-1} depth and $R_e\sim4.2$ Å equilibrium intermolecular distance,[5,56] as shown in Fig. 9(b). Interestingly, the R_e of the anisotropic potential is ~1 Å greater than the R_e of the isotropic potential. This difference is important because any realistic calculation of the $|10\rangle/|1\pm1\rangle$ splitting of a $J=1/J=0$ pair must include computation of the renormalized expectation value $\langle\Psi(R)|B(R)|\Psi(R)\rangle$. The isotropic potential dominates at most R, so $\Psi(R)$ will reflect its properties. Because R_e(isotropic)$<R_e$(anisotropic), $\langle B\rangle$ will include a large contribution from the repulsive inner wall of $B(R)$.

We now consider multiple $J=1/J=0$ pairwise interactions in hcp solid parahydrogen. In the simplest model, there is a single $J=1$ molecule at the origin of an otherwise pure p-H_2 lattice [cf. Fig. 8(b)]. The pairwise isotropic potential terms are simply additive. To compute the anisotropic potential, we need to convert each of the pairwise terms $B(R)C_{20}(\omega)$ to a single space-fixed coordinate system. The most convenient space-fixed system is the hcp crystal frame with the z-axis parallel to the crystalline c axis. We use the transformation of coordinates[5]

$$C_{20}(\omega)=\sum_m C_{2\bar{m}}(\Omega)C_{2m}(\Omega_i), \tag{2}$$

where ω (Ω) is the orientation of the $J=1$ molecule in the pair (crystal) frame and Ω_i is the orientation of the pair axis in the crystal frame. We sum over all sites $i\neq0$ to obtain the anisotropic potential of the pure crystal

$$V_{\text{anis.}}^{\text{p.c.}}=\sum_i\sum_m B(R_i)C_{2m}(\Omega_i)C_{2\bar{m}}(\Omega). \tag{3}$$

Because of hcp symmetry, the crystal sum over lattice sites i is only nonvanishing for $m=0$.[21] Therefore,

$$V_{\text{anis.}}^{\text{p.c.}}=\sum_i [B(R_i)C_{20}(\Omega_i)]C_{20}(\Omega)\equiv\epsilon_{2c}C_{20}(\Omega). \tag{4}$$

In an hcp crystal with a single nn intermolecular distance, the crystal sum in Eq. (4) vanishes for the first two shells of $J=0$ neighbors.[57] Because of this ''accidental cancellation'' and the rapid falloff of $|B(R)|$ with increasing R, the crystal field parameter ϵ_{2c} is small. For an isolated o-H_2 impurity in solid parahydrogen, $\epsilon_{2c}=0.0118$ cm^{-1}.[18]

The strongest transitions in the isotopic impurity $Q_1(0)$ infrared spectra should be those of nn $J=1/J=0$ o-D_2 or $J=1/J=0$ HD impurity pairs, as shown in Figs. 7(c) and 8(c). We consider a single nn impurity pair in a crystal of otherwise pure hcp parahydrogen. This is a reasonable approximation in the low impurity concentration limit. The $J=1$ molecule lies at the lattice origin and the isotopic impurity sits at site 1. The anisotropic potential for this impurity crystal is

$$V_{\text{anis.}}^{\text{i.c.}}=B_{D_2}(R_1)C_{20}(\omega)+\sum_{i\neq1}\sum_m B_{H_2}(R_i)C_{2m}(\Omega_i)C_{2\bar{m}}(\Omega), \tag{5}$$

where $B_{D_2}(R_1)$ and $B_{H_2}(R_i)$ are the respective anisotropic potential parameters for $J=1/o$-D_2 and $J=1/p$-H_2 pairs with intermolecular distances R_1 and R_i, and ω and Ω are the orientations of the $J=1$ molecule in the impurity pair and crystal frames, respectively. The potential has been written for a D_2 impurity but an equivalent expression could be written for an HD impurity. We note, that a $J=1/J=0$ impurity pair containing $J=1$ o-H_2 will have a somewhat different anisotropic potential parameter than the analogous pair containing $J=1$ p-D_2. Also, the potential parameters depend on the vibrational states of the impurity pair molecules.

The anisotropic potential can be written more conveniently by adding and subtracting a $v=0$ p-H_2 molecule at the isotopic impurity site. This leads to the expression

$$V_{\text{anis.}}^{\text{i.c.}}=[B_{D_2}(R_1)-B_{H_2}(R_1)]C_{20}(\omega)+\epsilon_{2c}C_{20}(\Omega)\equiv\Delta BC_{20}(\omega)+\epsilon_{2c}C_{20}(\Omega), \tag{6}$$

which is a convenient form because the impurity crystal anisotropic potential is divided into two terms with distinct

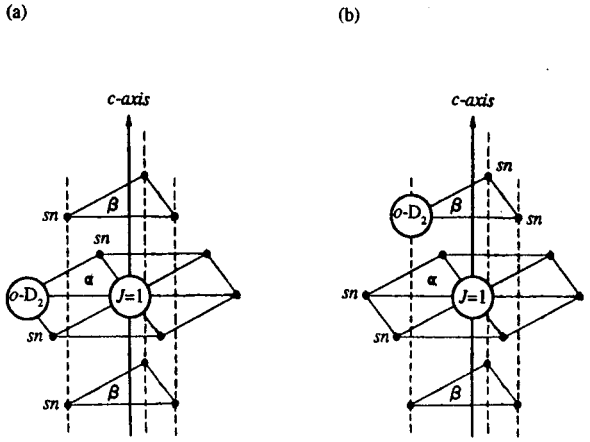

FIG. 10. In-plane (ip) and out-of-plane (oop) impurity pair configurations (Ref. 5). In these diagrams, sections of three neighboring basal planes of a hexagonal close-packed (hcp) lattice are presented, with the black dots representing p-H_2 molecules. Nearest-neighbor (nn) molecules in the same basal plane are connected by solid lines and a bold arrowed line marks the unique c axis of the crystal. The planes are packed $\alpha\beta\alpha\beta$, as can be seen by the dotted traces connecting molecules in the β planes. In (a), the lattice contains a nn ip $J=1/o$-D_2 impurity pair and in (b), the lattice contains a nn oop $J=1/o$-D_2 impurity pair. The impurity pair molecules share four nn which are marked as ''sn''.

angular dependences, the *impurity pair term* $[\Delta B C_{20}(\omega)]$ and the *pure crystal term* $[\epsilon_{2c} C_{20}(\Omega)]$. The ΔB term represents the *difference* in anisotropic interactions between a $J=1/o$-D_2 and a $J=1/p$-H_2 impurity pair. In general, ΔB will have contributions from the changes in both the *potential B(R) and renormalization* $\langle B\rangle$ which accompany isotopic substitution.

In the experimental isotopic impurity $Q_1(0)$ spectrum, the frequency spacings between the strong lines were typically $\sim 0.1\ \mathrm{cm}^{-1}$. This was an order of magnitude larger than $|\epsilon_{2c}|$ and led us to postulate that these large splittings were mainly due to ΔB, i.e., $|\Delta B| \gg |\epsilon_{2c}|$ for nn impurity pairs. This results in the qualitative energy diagrams shown in Figs. 7(c) and 8(c). For nn impurity pairs, the $\Delta B C_{20}(\omega)$ term quantizes the $|1M\rangle$ states along the impurity pair axis. The crystal field term $\epsilon_{2c} C_{20}(\Omega)$ acts as a small perturbation on these states, whose most noticeable effect is splitting the degenerate $|1\pm1\rangle$ states into the nondegenerate linear combinations of states, $|11_+\rangle$ and $|11_-\rangle$. There is a single symmetry element of the impurity pair crystal, a mirror plane, and the ''+'' and ''−'' denote the reflection symmetry of these linear combination states. There is an added complication because nn impurity pairs exist in two geometric configurations, as shown in Fig. 10. In the in-plane (ip) configuration, both impurities lie in the same basal plane, which is also the symmetry plane. In the out-of-plane (oop) configuration, the impurities lie in adjacent basal planes and the symmetry plane is defined by the impurity pair axis and the c axis.

With the appropriate transformations of coordinates of Eq. (6) and the postulated impurity pair $|1M\rangle$ states, we derive the first order energy eigenvalue expression

TABLE III. First order energies of nearest-neighbor impurity pairs.[a]

	In-plane		Out-of-plane	
$\lvert 1M\rangle$ State	C_1	C_2	C_1	C_2
$\lvert 10\rangle$	+2/5	−1/5	+2/5	+1/5
$\lvert 11_+\rangle$	−1/5	−1/5	−1/5	0
$\lvert 11_-\rangle$	−1/5	+2/5	−1/5	−1/5

[a]The first order energy expression is: $E=C_1\Delta B+C_2\epsilon_{2c}$, where C_1 and C_2 are the tabulated constants, and ΔB and ϵ_{2c} are the anisotropic potential parameters.

$$E = C_1 \Delta B + C_2 \epsilon_{2c}, \tag{7}$$

where values of C_1 and C_2 for ip and oop nn impurity pairs are listed in Table III. The correct second order expressions are given in Sec. VI A 2.

Equations (6) and (7) were derived in the context of nn impurity pairs but also hold for more distant pairs. However, ΔB decays strongly with increasing impurity pair distance whereas ϵ_{2c} is independent of this distance [cf. Eqs. (5) and (7)]. For more distant impurity pairs, $|\Delta B|$ will be comparable or smaller than $|\epsilon_{2c}|$, and the pair states and energies will be quite different from those of nn impurity pairs. We derive the energy expressions for next nearest-neighbor (nnn) pairs in Sec. VI A 2.

C. Intensity calculations

We consider a $J=1$ molecule at the lattice origin and a $J=0$ isotopic impurity at site i. The $Q_1(0)$ transition dipole moment of this single pair is[36]

$$\mu_\kappa = \sqrt{15}(Q\alpha_{01}/R_i^4)\sum_m (-1)^m C(123;-\kappa,m) \times C_{3,\kappa-m}(\Omega_i) C_{2m}(\Omega), \tag{8}$$

where $\kappa=0,\pm1$ (parallel, perpendicular polarization), Q is the $v=0$ permanent quadrupole moment of the $J=1$ molecule, α_{01} is the $v=1\leftarrow0$ transition isotropic polarizability ($\langle v=1|\alpha|v=0\rangle$) of the isotopic impurity, R_i is the pair intermolecular distance, $C(123;-\kappa,m)$ is a Clebsch–Gordan coefficient, and Ω_i and Ω are the respective orientations of the impurity pair axis and $J=1$ internuclear axis in some reference frame. The R^{-4} dependence of the dipole moment implies a R^{-8} dependence of the intensity. For nn impurity pairs, Table IV lists the numerically calculated relative $Q_1(0)$ intensities.[24,51] The $|1M\rangle$ states are those derived in Secs. IV A and IV B.

D. Quadrupolar line broadening

In other papers,[35,47] we discuss in much greater detail the theory of inhomogeneous broadening due to quadrupolar interactions. At this time, we simply state the results of our analysis in these papers, and then use these results as an aid in spectral assignment and analysis.

The allowed impurity pair $Q_1(0)$ transitions can be grouped into two categories, those in which the impurity pair $J=1$ molecule does not change its orientation ($\Delta M=0$) and

TABLE IV. Crystal frame[a] relative intensities of nearest-neighbor impurity pair $Q_1(0)$ transitions.

	Relative intensity[c]			
	nn ip[d]		nn oop	
Transition[b]	∥	⊥	∥	⊥
$\|10\rangle \leftarrow \|10\rangle$	0	48	64	16
$\|11_+\rangle \leftarrow \|11_+\rangle$	0	12	16	4
$\|11_-\rangle \leftarrow \|11_-\rangle$	0	12	16	4
$\|11_-\rangle \leftarrow \|11_+\rangle$	0	0	0	0
$\|11_+\rangle \leftarrow \|11_-\rangle$	0	0	0	0
$\|11_+\rangle \leftarrow \|10\rangle$	0	12	8	8
$\|10\rangle \leftarrow \|11_+\rangle$	0	12	8	8
$\|11_-\rangle \leftarrow \|10\rangle$	24	0	0	12
$\|10\rangle \leftarrow \|11_-\rangle$	24	0	0	12

[a]The experimental intensities can be directly compared to these calculated intensities.
[b]The $1M\rangle$ states are those derived in Secs. IV A and IV B.
[c]In these calculations, it was assumed that the 4.2 K thermal energy is much larger than any of the $|1M\rangle$ splittings, and therefore, each of the ground state levels has the same thermal population.
[d]Abbreviations: nn—nearest-neighbor, ip—in-plane, oop—out-of-plane, ∥—parallel, ⊥—perpendicular.

those in which it does change its orientation ($\Delta M \neq 0$). The transitions $|10\rangle \leftarrow |10\rangle$, $|11_\pm\rangle \leftarrow |11_\pm\rangle$ fall into the former category and the transitions $|10\rangle \leftarrow |11_\pm\rangle$, $|11_\pm\rangle \leftarrow |10\rangle$ fall into the latter category. Qualitatively, our analysis shows that these two different categories of transitions experience very different amounts of quadrupolar broadening. Because of this effect, we expect that the $\Delta M \neq 0$ transitions are much broader than the $\Delta M = 0$ transitions.

V. $Q_1(0)$ SPECTRAL ASSIGNMENT

A. Nearest-neighbor *o*-H_2 induced transitions of D_2 and HD

As shown in Fig. 3, we discriminate between *o*-H_2 induced and *p*-D_2 induced $Q_1(0)$ transitions by comparing the spectra of different crystals with varying [*o*-H_2] and [*p*-D_2]. For more specific assignment, we use the qualitative nn impurity pair energy diagrams in Figs. 7(c) and 8(c) and the calculated transition intensities in Table IV. With these tools, we are able to assign all of the strong *o*-H_2 induced lines in the impurity D_2 and HD $Q_1(0)$ spectra as specific quantum state transitions of *o*-H_2/*o*-D_2 and *o*-H_2/HD nn impurity pairs, respectively. These assignments are listed in Tables I and II and fit combination differences which agree to within 5×10^{-4} cm^{-1}, the instrumental precision. Except for the $|10\rangle \leftarrow |10\rangle$ transition, the ip and oop transitions are resolved from one another. These comprehensive assignments give a complete set of $Q_1(0)$ energy diagrams for *o*-H_2/*o*-D_2 and *o*-H_2/HD nn impurity pairs in solid parahydrogen, as presented in Figs. 11(a) and 11(b). These are self-consistent assignments because all of the most intense transitions in the experimental spectra are accounted for in the nn impurity pair model of Sec. IV, and vice versa. The assignments have additional confirmation by the near perfect agreement between experimental and calculated intensity polarization dependences. Also, the total integrated intensity of the nn *o*-H_2 induced $Q_1(0)$ transitions of either D_2 or HD is $\sim2\times10^{-14}$ cm^3/s, in agreement with the theoretical value of Sears and Van Kranendonk.[36] Finally, the $\Delta M \neq 0$ ($|10\rangle \leftarrow |11_\pm\rangle, |11_\pm\rangle \leftarrow |10\rangle$) transitions are two times broader than their $\Delta M = 0$ ($|10\rangle \leftarrow |10\rangle, |11_\pm\rangle \leftarrow |11_\pm\rangle$) counterparts (cf. Fig. 4), consistent with the models for the impurity pair states and for $Q_1(0)$ quadrupolar broadening (cf. Sec. IV D).

B. Nearest-neighbor *p*-D_2 induced transitions of D_2

In the concentration dependence studies presented in Fig. 3, the two groups of *o*-D_2 $Q_1(0)$ lines at 2986.94 and 2984.84 cm^{-1} were assigned as *p*-D_2 induced transitions. By comparison with both the nn *o*-H_2/*o*-D_2 $Q_1(0)$ assignment and with the calculated intensities in Table IV, the strong higher and lower frequency *p*-D_2 induced transitions can be respectively assigned as specific $|11_\pm\rangle \leftarrow |11_\pm\rangle$ and $|10\rangle \leftarrow |10\rangle$ $Q_1(0)$ transitions of *p*-D_2/*o*-D_2 nn impurity pairs. These assignments are listed in Table I. The assigned $|11_\pm\rangle \leftarrow |11_\pm\rangle$ transitions happen to overlap with the more distant pair $J=1$/*o*-D_2 $Q_1(0)$ transitions. This overlap is known because the transition frequencies of these more distant pairs should be clustered around the isolated *o*-D_2 $Q_1(0)$ transition frequency at 2986.9434 cm^{-1}.[13,48,49] The *p*-D_2 induced nn transitions were discriminated by their strong dependence on the *p*-D_2 concentration of the crystal. Also, the polarization dependences of the experimental ip and oop $|11_\pm\rangle \leftarrow |11_\pm\rangle$ intensities match those calculated from the impurity pair model. Interestingly, the nn ip and oop *p*-D_2 induced $|10\rangle \leftarrow |10\rangle$ transitions were split by ~100 MHz. This is in marked contrast to the analogous nn *o*-H_2 induced $|10\rangle \leftarrow |10\rangle$ transitions of *o*-D_2 and HD, for which there was no detectable ip/oop splitting.

All of the assigned *p*-D_2/*o*-D_2 nn impurity pair $Q_1(0)$ transitions are the sharper, more intense $\Delta M = 0$ type. We have not yet definitely observed the weaker *p*-D_2/*o*-D_2 $\Delta M \neq 0$ transitions, $|10\rangle \leftarrow |11_\pm\rangle$ and $|11_\pm\rangle \leftarrow |10\rangle$, and therefore, could not assign single nn *p*-D_2/*o*-D_2 $|11_\pm\rangle \leftarrow |11_\pm\rangle$ lines as specifically either the $|11_+\rangle \leftarrow |11_+\rangle$ or the $|11_-\rangle \leftarrow |11_-\rangle$ transitions.

C. Next-nearest-neighbor *o*-H_2 induced transitions of D_2 and HD

Compared to the $Q_1(0)$ transitions of nn impurity pairs, the transitions of more distant pairs should have much weaker intensities [cf. Eq. (8)] as well as much smaller frequency splittings (cf. Sec. IV B). As impurity pair distance increases, the impurity pair $Q_1(0)$ frequencies should also tend toward the isolated isotopic impurity $Q_1(0)$ frequency, 2986.9434 cm^{-1} for D_2. In the D_2 $Q_1(0)$ spectra, there was a cluster of weak lines around this frequency, most of which

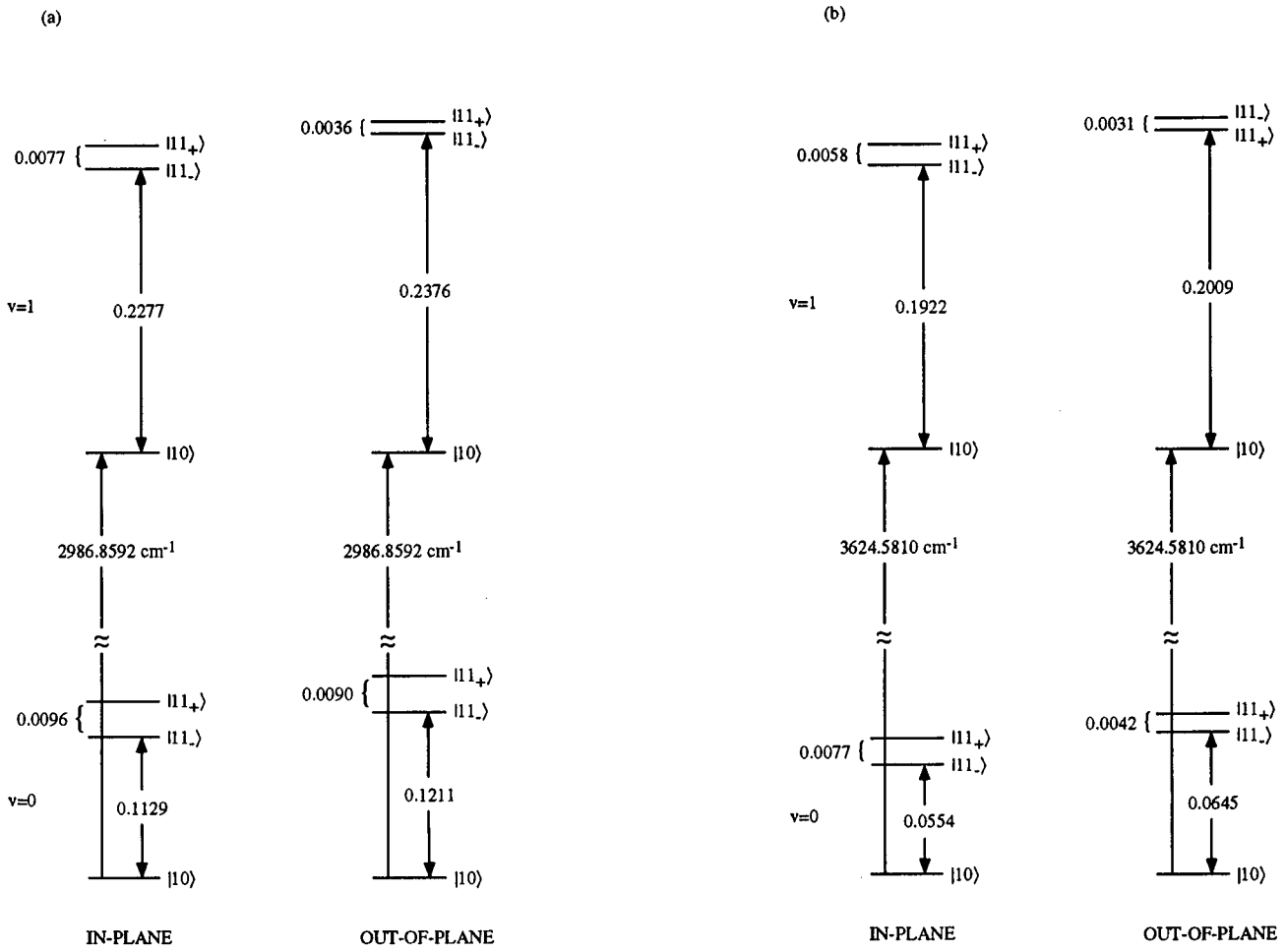

FIG. 11. $Q_1(0)$ energy level diagrams for (a) o-H_2/o-D_2 and (b) o-H_2/HD nearest-neighbor impurity pairs in solid parahydrogen. All energies are in cm^{-1}. In (a), the energy spacings are derived from the spectra of a sample containing 0.25% o-D_2, 0.2% o-H_2, 0.04% HD, and 0.01% p-D_2 impurities. In (b), the energy spacings are derived from spectra of a sample containing 0.24% HD and 0.2% o-H_2 impurities. The states are labeled by the $|1M\rangle$ orientation of the o-H_2 impurity pair molecule, and this orientation is quantized relative to the impurity pair intermolecular axis. The ''in-plane'' and ''out-of-plane'' impurity pair configurations have slightly different energy spacings.

we assign as more distant impurity pair $Q_1(0)$ transitions. These features are shown in Fig. 12(a). In this particular crystal, the o-H_2 induced features were dominant because $[o\text{-}H_2]/[p\text{-}D_2]\sim 20$. This frequency region also contained previously assigned nn p-D_2 induced $|11_{\pm}\rangle\leftarrow|11_{\pm}\rangle$ features.

The isolated impurity HD $Q_1(0)$ transition frequency has not yet been measured, but 3624.68 cm^{-1} is a good estimate (cf. Sec. VI A 1). Figure 12(b) shows the group of spectral lines around this frequency which we assign as the more distant impurity pair transitions of HD. The more distant pair spectra of D_2 and HD have marked similarity, as might be expected.

In Fig. 12, the marked transitions at 2986.9348 and 3624.6695 cm^{-1} are assigned as the o-H_2 induced $|10\rangle\leftarrow|10\rangle$ nnn (next nearest-neighbor) $Q_1(0)$ transitions of D_2 and HD, respectively. There are several arguments which lead to these assignments. In the impurity pair model, the nnn transitions should be the most intense distant neighbor $Q_1(0)$ features, with $\sim$1/32 of the nn intensity. This ratio is calculated from the relative numbers of nnn to nn pairs (6:12), the relative impurity pair intermolecular distances ($R_{nnn}=\sqrt{2}R_{nn}$), and the R^{-8} intensity dependence of $Q_1(0)$ transitions [cf. Eq. (8)]. Of all the more distant pair transitions, the nnn features should also have the largest spectral splittings because of the rapid decrease in $|\Delta B|$ with impurity pair separation. The nnn energy level pattern should be similar to that of the nn, except for a diminished $|10\rangle/|11_{\pm}\rangle$ splitting due to a smaller ΔB. The marked transitions in Fig. 12 are the strongest sharp transitions on the low frequency side of this more distant neighbor spectral region, as one would expect for the nnn $|10\rangle\leftarrow|10\rangle$ transition. Additionally, these features are $\sim$1/50 as intense as the analogous nn impurity pair transitions and do not have a strong polarization dependence, in agreement with theoretical predictions.[24,51] Furthermore, we have been able to completely assign the other nnn o-H_2/HD $Q_1(0)$ transitions, as listed in Table II. These nnn assignments are more tentative than the nn assignments, but do fit combination differences, as well as follow the predicted intensity polarization dependences.[24,51] The nnn o-H_2/HD $Q_1(0)$ energy diagram is presented in Fig. 13 and is similar to that for the nn, except for a much smaller $|10\rangle/|11_{\pm}\rangle$ splitting. The nnn have a single geometric configuration.

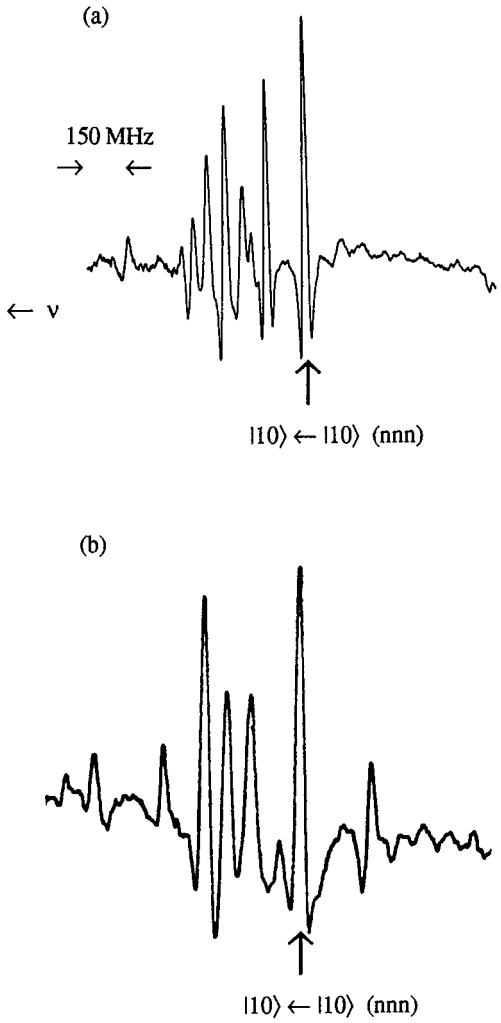

FIG. 12. $Q_1(0)$ spectra of more distant impurity pairs. Parahydrogen crystal (a) contained 0.25% o-D_2, 0.2% o-H_2, and 0.01% p-D_2 impurities, while crystal (b) contained 0.24% HD and 0.2% o-H_2 impurities. Traces (a) and (b) are tone-burst modulated spectra spanning $\sim$0.05 cm^{-1} regions about 2986.94 and 3624.67 cm^{-1}, respectively. In both scans, the frequency scales are approximately the same and the laser polarization is perpendicular to the crystalline c axis. The marked features in traces (a) and (b) are assigned as the $|10\rangle \leftarrow |10\rangle$ transitions of o-H_2/o-D_2 and o-H_2/HD next nearest-neighbor impurity pairs, respectively.

D. Weaker spectral features and triples

The $Q_1(0)$ regions of D_2 and HD each had $\sim$100 additional weaker lines, most of which were found in the $\sim$0.4 cm^{-1} frequency interval which also contained the strong nn impurity pair transitions. In the case of D_2, a few of these lines can be assigned as $Q_1(1)$ transitions of nn p-D_2/o-H_2 or p-D_2/p-D_2 impurity pairs.[58] The rest of the features are likely the $Q_1(0)$ transitions of impurity triples and perhaps larger clusters of impurities. For HD, there are two triple permutations, $J=1$ o-H_2/$J=1$ o-H_2/$J=0$ HD and $J=1$ o-H_2/$J=0$ HD/$J=0$ HD, and each permutation has several different nn geometric configurations. The D_2 spectra have the additional complication of triples containing $J=1$ p-D_2. The nn triples transitions are weaker than nn pair transitions because at low impurity concentrations, the statistical probability of a particular impurity configuration decreases with the number of impurities in the configuration. The pattern of these weaker lines is strikingly similar in the D_2 and HD spectra. This pattern is defined by their frequencies relative to those of the nn impurity pair $Q_1(0)$ transitions, by the polarization dependences of their intensities, and by their linewidths. Figure 14 shows one example of this remarkable pattern similarity. This similarity indicates that the states and energies of a given triple configuration containing o-D_2 are much like those of the analogous triple configuration containing HD. A more rigorous analysis of the triples' spectra is not yet done.

VI. DISCUSSION

A. $Q_1(0)$ spectral fitting and analysis

1. Average frequencies and isotropic interactions

We have been able to rigorously assign all of the $Q_1(0)$ transitions of o-H_2/o-D_2 and o-H_2/HD nn impurity pairs. We now combine the experimental results with the impurity pair model and obtain quantitative parameters which describe the isotropic intermolecular interactions. Using the experimental nn o-H_2/o-D_2 transition frequencies from Table I and derived infrared forbidden $|11_{\pm}\rangle \leftarrow |11_{\mp}\rangle$ transition frequencies from Fig. 11(a), we calculate an average experimental nn o-H_2/o-D_2 $Q_1(0)$ frequency of 2986.9351 cm^{-1}. This average frequency is compared to the experimental $Q_1(0)$ frequency of isolated o-D_2 molecules in the parahydrogen crystal, 2986.9434 cm^{-1}.[13,48,49] The difference in the average $Q_1(0)$ frequency of isolated D_2 and nn impurity pair D_2 is $\sim$0.008 cm^{-1}, too large to be attributed to a matrix shift difference between the different crystals used in the different experiments. This average frequency difference must result from the difference in isotropic interactions between $J=0/J=0$ (p-H_2/o-D_2) and $J=1/J=0$ (o-H_2/o-D_2) pairs [cf. Figs. 7(b) and 7(c)].

One important difference between a $J=1$ and a $J=0$ molecule is that the former has a rotationally averaged quadrupole moment while the latter does not. This leads to larger induction and second order EQQ interactions of $J=1/J=0$ pairs relative to their $J=0/J=0$ counterparts. The induction term for a $J=1/J=0$ pair scales linearly with the vibrationally dependent $J=0$ molecular polarizability[5] and the second order EQQ interaction scales approximately as $-\Gamma^2/B_{\rm rot}$, where Γ is the nn quadrupolar coupling constant ($\sim$0.6 cm^{-1}) and $B_{\rm rot}$ is the $J=0$ rotational constant. Each interaction increases the binding energy of a nn o-H_2/o-D_2 pair by $\sim$0.1 cm^{-1} relative to its p-H_2/o-D_2 counterpart.[5,24,51] This binding energy increase is $\sim$6% larger when the D_2 is vibrationally excited and results in a $\sim$0.012 cm^{-1} decrease in the average $Q_1(0)$ vibrational frequency of a nn o-H_2/o-D_2 impurity pair relative to that of an isolated o-D_2 impurity. This theoretical frequency difference has the same sign and approximate magnitude as the experimental one, 0.008 cm^{-1}. To obtain more accurate experimental results, we should measure the $Q_1(0)$ frequencies of isolated and impurity pair D_2 for the same crystal. The D_2

TABLE V. Experimental anisotropic potential parameters of o-H_2/o-D_2 and o-H_2/HD impurity pairs.

Pair type[a]	Isotopic impurity	ΔB (cm^{-1})	ΔB_{diff} (cm^{-1})[b]	ϵ_{2c} (cm^{-1})	$\Delta\epsilon_{2c}$ (cm^{-1})[c]
nn ip	$v=0$ D_2	−0.2042	+0.0227	−0.160	−0.0042
nn oop	$v=0$ D_2	−0.2269		+0.0400	+0.0518
nn ip	$v=1$ D_2	−0.3923	+0.0152	−0.0128	−0.0010
nn oop	$v=1$ D_2	−0.4075		+0.0175	+0.0293
nn ip	$v=0$ HD	−0.1052	+0.0142	−0.0128	−0.0010
nn oop	$v=0$ HD	−0.1194		+0.0189	+0.0307
nn ip	$v=1$ HD	−0.3300	−0.008	−0.0097	+0.0021
nn oop	$v=1$ HD	−0.3292		−0.0160	−0.0042
nnn	$v=0$ HD	−0.0134		+0.0030	+0.0148
nnn	$v=1$ HD	−0.0286		+0.0089	+0.0207

[a]Abbreviations: nn—nearest-neighbor, nnn—next-nearest-neighbor, ip—in-plane, oop—out-of-plane.
[b]$\Delta B_{diff}=|\Delta B_{oop}|-|\Delta B_{ip}|$ [Eq. (15)].
[c]$\Delta\epsilon_{2c}=\epsilon_{2c}^{ic}-\epsilon_{2c}^{pc}$ [Eq. (16)], where ϵ_{2c}^{ic} is tabulated in the previous column and $\epsilon_{2c}^{pc}=-0.0118$ cm^{-1} (cf. Ref. 18).

concentration should be minimized to reduce vibrational coupling effects on the isolated D_2 vibrational frequency.

The average experimental nn o-H_2/HD $Q_1(0)$ vibrational frequency is 3624.6716 cm^{-1}. The isolated HD impurity $Q_1(0)$ frequency has not yet been measured. By analogy with D_2, the isolated HD frequency should be ~3624.68 cm^{-1}.

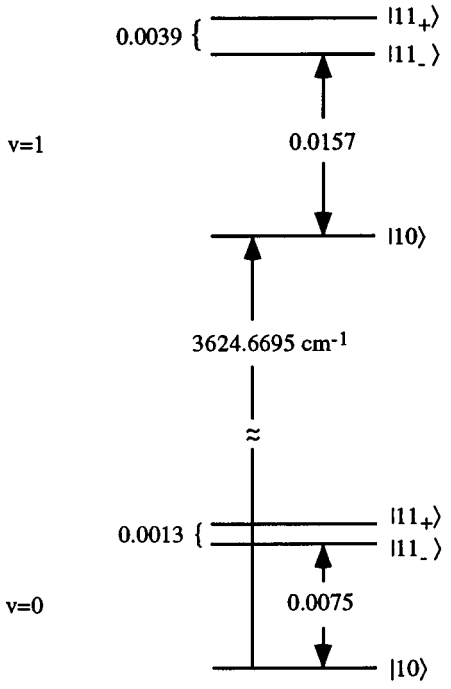

FIG. 13. $Q_1(0)$ energy level diagram for o-H_2/HD next nearest-neighbor impurity pairs in solid parahydrogen. All energies are in cm^{-1}. The energy spacings were derived from the spectra of a sample containing 0.24% HD and 0.2% o-H_2 impurities. The states are labeled by the $|1M\rangle$ orientation of the o-H_2 impurity pair molecule, and this orientation is quantized relative to the impurity pair intermolecular axis.

The average $Q_1(0)$ frequency of nnn o-H_2/HD pairs is 3624.6758 cm^{-1}. Compared to nn pairs, the nnn pairs have an average $Q_1(0)$ frequency which is closer to that of isolated HD impurities. This is a result of the smaller induction and second order EQQ interactions of nnn impurity pairs relative to those of nn pairs. Average frequency analysis can also be applied to other $Q_v(0)$ parahydrogen spectra, such as the $Q_3(0)$ spectra.[13,17]

We have observed that the p-D_2 induced $|10\rangle\leftarrow|10\rangle$ and $|11_\pm\rangle\leftarrow|11_\pm\rangle$ transitions are red shifted ~0.03 cm^{-1} relative to their o-H_2 induced counterparts (cf. Fig. 3). This is counter to the vibrational coupling arguments of Chan[46] which predicted that the $Q_1(0)$ vibrational frequency of a nn p-D_2/o-D_2 impurity pair would be blue shifted by ~0.016 cm^{-1} relative to that of a nn o-H_2/p-D_2 impurity pair. The experimental 0.03 cm^{-1} red shift probably arises from the larger isotropic interactions around a D_2 molecule relative to those around an H_2 molecule. These increased interactions result from the smaller zero-point motion of heavier D_2 relative to lighter H_2.[2,10] The immediate environment of a nn p-D_2/o-D_2 impurity pair should have a smaller R_0 and more localized molecular motion than its o-H_2/o-D_2 counterpart. As can be seen in Fig. 9(a), this should lead to increased binding energy for the p-D_2/o-D_2 impurity pair because the decreased R_0 will be closer to the R_e of the isotropic potential and because the smaller zero-point motion will give less weight to short intermolecular separations at which the isotropic potential is repulsive.

2. Splittings and anisotropic interactions

Figure 11 shows that the nn $|10\rangle/|11_\pm\rangle$ energy level splittings are much larger than the $|11_+\rangle/|11_-\rangle$ splittings. This is consistent with the inequality $|\Delta B|\gg|\epsilon_{2c}|$, where we refer to the terms of the impurity crystal anisotropic potential in Eq. (6) and to the first order impurity pair energies of Eq. (7). In other words, replacement of a nn $J=0$ H_2 by a $J=0$ D_2 or HD (the ΔB term) makes a much greater contribution to the

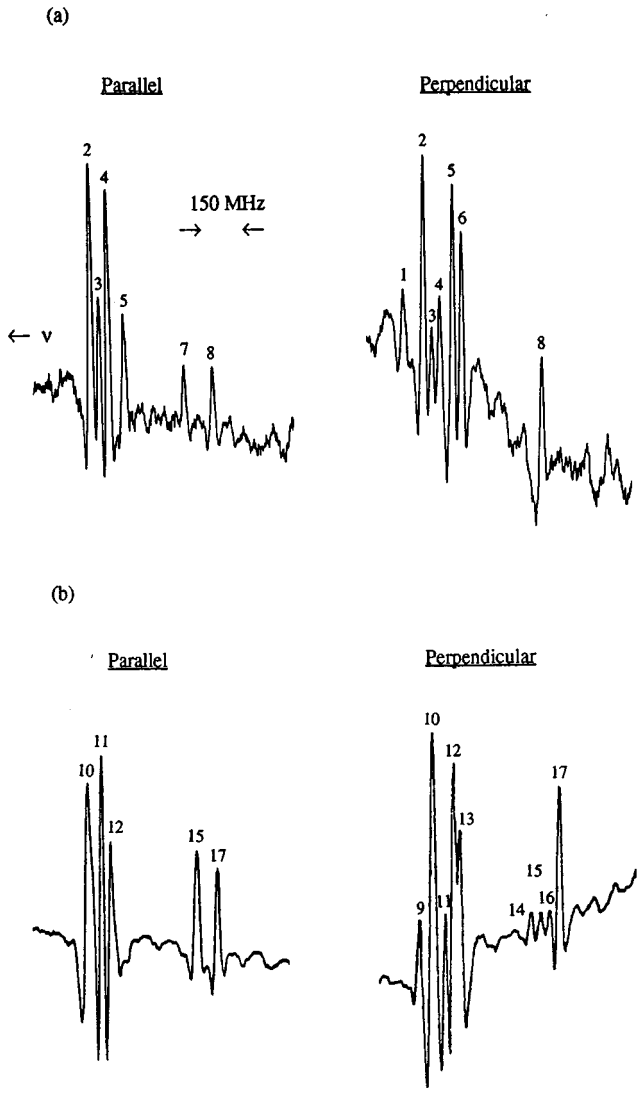

FIG. 14. Pattern similarity of the weaker features in the D_2 and HD $Q_1(0)$ spectra. Parahydrogen crystal (a) contained 0.25% o-D_2, 0.2% o-H_2, 0.04% HD, and 0.01% p-D_2 impurities, while crystal (b) contained 0.24% HD and 0.2% o-H_2 impurities. The traces in (a) and (b) are tone-burst modulated spectra spanning $\sim$0.03 cm^{-1} regions about 2986.71 and 3624.43 cm^{-1}, respectively. These regions are 0.15 cm^{-1} to lower frequency of the $|10\rangle \leftarrow |10\rangle$ transitions of o-H_2/o-D_2 and o-H_2/HD nearest-neighbor impurity pairs, respectively. Spectra with different polarizations are presented and the frequency scales are approximately the same in all scans. There is striking pattern similarity in the weaker features of the D_2 and HD spectra, where the pattern is described by the observed frequencies, polarization dependences, and linewidths. In the displayed scans, the following pairs of D_2, HD peaks form a pattern: 1,9; 2,10; 4,11; 5,12; 6,13; 7,15; 8,17. The HD analog of peak 3 may be an unresolved shoulder of peak 10.

anisotropic potential than does the pure crystal field (the ϵ_{2c} term). Equation (7) is ''exact'' for nn ip pairs because the ip $|10\rangle$, $|11_{\pm}\rangle$ states are eigenstates of both potential terms $\Delta B C_{20}(\omega)$ and $\epsilon_{2c} C_{20}(\Omega)$. For nn oop pairs, the impurity pair axis and crystalline c axis are not orthogonal and the $\epsilon_{2c} C_{20}(\Omega)$ term slightly mixes the $|10\rangle$ and $|11_{+}\rangle$ states. To account for this mixing, we diagonalize the potential matrix for the oop states

$$\begin{pmatrix} (2\Delta B+\epsilon_{2c})/5 & i\sqrt{2/25}\,\epsilon_{2c} \\ -i\sqrt{2/25}\,\epsilon_{2c} & -\Delta B/5 \end{pmatrix}, \tag{9}$$

where row/column 1 (2) is for the $|10\rangle$ ($|11_{+}\rangle$) state. The corrected oop energies are

$$\begin{aligned} E_{10} &= (1/10)\{\Delta B+\epsilon_{2c}+\sqrt{9(\Delta B+\epsilon_{2c})^2-12\Delta B\epsilon_{2c}}\}, \\ E_{11_+} &= (1/10)\{\Delta B+\epsilon_{2c}-\sqrt{9(\Delta B+\epsilon_{2c})^2-12\Delta B\epsilon_{2c}}\}, \\ E_{11_-} &= -(1/5)\{\Delta B+\epsilon_{2c}\}. \end{aligned} \tag{10}$$

Using Eqs. (7) and (10), we derive expressions for ΔB and ϵ_{2c},

$$\begin{aligned} \Delta B_{\mathrm{ip}} &= (5/3)\{E_{10}-E_{11_+}\}, \\ \epsilon_{2c_{\mathrm{ip}}} &= (5/3)\{E_{11_-}-E_{11_+}\}, \end{aligned} \tag{11a}$$

$$\begin{aligned} \Delta B_{\mathrm{oop}} &= (5/6)\{\Delta E'+\Delta E'' \\ &\quad -\sqrt{(\Delta E'+\Delta E'')^2-12\Delta E'\Delta E''}\}, \\ \epsilon_{2c_{\mathrm{oop}}} &= (5/6)\{\Delta E'+\Delta E'' \\ &\quad +\sqrt{(\Delta E'+\Delta E'')^2-12\Delta E'\Delta E''}\}, \end{aligned} \tag{11b}$$

where $\Delta E' = E_{10} - E_{11_-}$ and $\Delta E'' = E_{11_+} - E_{11_-}$. Inserting the experimental nn impurity pair splittings from Fig. 11, we derive values of ΔB and ϵ_{2c} for o-$H_2/v=0,1$ o-D_2 and o-$H_2/v=0,1$ HD nn impurity pairs (cf. Table V). We do not learn about the uncertainties of these two parameters because there are only two splittings for each kind of pair. Depending on the pair, $|\Delta B|$ is a factor of 5 to 40 times larger than the $|\epsilon_{2c}|$. For oop pairs, there is at most 10% mixing between the $|10\rangle$ and the $|11_{+}\rangle$ states. This has a minor effect on the calculated $Q_1(0)$ intensities.

For nnn pairs, the impurity pair axis and crystalline c axis are not orthogonal and we again need to consider the mixing of the $|10\rangle$ and $|11_{+}\rangle$ states. After taking into account the different pair axis orientations, the nnn and nn oop derivations are analogous. We obtain

$$\begin{aligned} \Delta B_{\mathrm{nnn}} &= (5/6)\{\Delta E'+\Delta E'' \\ &\quad -\sqrt{(\Delta E'+\Delta E'')^2-6\Delta E'\Delta E''}\}, \\ \epsilon_{2c_{\mathrm{nnn}}} &= (5/6)\{\Delta E'+\Delta E'' \\ &\quad +\sqrt{(\Delta E'+\Delta E'')^2-6\Delta E'\Delta E''}\}. \end{aligned} \tag{12}$$

The parameter values for o-H_2/HD nnn impurity pairs are listed in Table V and are derived from the energy level splittings of Fig. 13. The nnn $|\epsilon_{2c}|$ are at least three times smaller than the nnn $|\Delta B|$, giving about 10% mixing of the nnn $|10\rangle$ and $|11_{+}\rangle$ states.

B. Interpretation of the anisotropic potential parameters

In our discussion of the experimental anisotropic potential parameters, we only consider o-H_2/o-D_2 and o-H_2/HD

impurity pairs because we do not yet have adequate spectral information to obtain anisotropic potential parameters for impurity pairs containing $J=1$ p-D_2.

1. Nearest-neighbor ΔB parameter

The ΔB parameter includes contributions to the anisotropic potential from replacement of one $J=0$ p-H_2 molecule by a $J=0$ o-D_2 or HD molecule [cf. Eq. (6)]. For all impurity pairs, ΔB is negative and $|\Delta B|$ increases upon vibrational excitation of the $J=0$ isotopic impurity (cf. Table V). Also, for a given nn pair type and isotopic impurity vibrational state, $|\Delta B_{D_2}| > |\Delta B_{HD}|$, where the subscript is the $J=0$ isotopic molecule of the nn impurity pair. Qualitatively, the larger mass change accompanying substitution of heavier D_2 has a greater effect on ΔB than do the new dipolar interactions introduced with substitution of lighter HD. These new dipolar interactions will be quite small because of the minsicule HD dipole moment, 6×10^{-4} D.[59]

The increase in $|\Delta B|$ which accompanies vibrational excitation of nn D_2 or HD is approximately proportional to $\mu^{-1/2}$, i.e.,

$$\Delta B_{vib}=|\Delta B_{v=1}|-|\Delta B_{v=0}|\propto\mu^{-1/2}, \tag{13}$$

where μ is the reduced mass of the D_2 or HD isotope. Numerically, ΔB_{vib} is ~0.18 cm^{-1} for D_2 and ~0.22 cm^{-1} for HD, comparable to $|\Delta B|$ for these isotopes. The $\mu^{-1/2}$ proportionality of ΔB_{vib} relates to the $\mu^{-1/2}$ v vibrational dependence of the hydrogenic molecular constants (polarizability, quadrupole moment, etc.).[5,50,60–62] ΔB may depend on these molecular constants in some nonlinear way. However, the vibrational dependences of these constants are small and enter linearly into the changes in $|\Delta B|$ which accompany impurity vibrational excitation. Hence, ΔB is proportional to $\mu^{-1/2}$ v (also confirmed by analysis of p-H_2 overtone spectra[13,17]).

We now compare the experimental ΔB to two calculations of ΔB. In the first approach, Byers and Oka computed the induction and second order EQQ (electric quadrupole–quadrupole) contributions to ΔB for o-H_2/o-D_2 and o-H_2/HD nn impurity pairs.[24,51] These interactions probably make smaller contributions to ΔB than does dispersion,[5] but their rigorous analytical expressions are more amenable to direct computation. In this model, the impurity pairs are embedded in a rigid hcp parahydrogen lattice with fixed nn intermolecular distance $R_0=3.783$ Å.[2] They calculate that $|\Delta B^{Ind}|$ is typically a few thousandths of a cm^{-1} and $|\Delta B^{2nd\ EQQ}|$ is typically a few hundredths of a cm^{-1}. $\Delta B^{2nd\ EQQ}$ is always negative and increases in magnitude by a factor of 1.5 to 2 upon vibrational excitation of the isotopic impurity. $|\Delta B^{2nd\ EQQ}|$ is larger for an o-$H_2/v=0,1$ o-D_2 pair relative to the respective o-$H_2/v=0,1$ HD pair.

These computational results make qualitative sense. For a $J=1/J=0$ nn pair, the induction and second order EQQ interactions make comparable contributions[8] to the pair anisotropic potential at $R=R_0$. To calculate ΔB, one must take the *difference* between the anisotropic interactions of a $J=1/J=0$ o-D_2 or $J=1/J=0$ HD pair relative to those of the analogous $J=1/J=0$, $v=0$ p-H_2 pair. Qualitatively, induction scales with the $J=0$ molecule's polarizability, whereas second order EQQ[8] scales as $-\Gamma^2/B_{rot}$, where Γ is the EQQ coupling constant (~0.6 cm^{-1})[7] and B_{rot} is the rotational constant of the $J=0$ molecule. The polarizability of a $J=0$, $v=0$ or 1 o-D_2 or HD differs from that of a $J=0$, $v=0$ p-H_2 by at most 7%,[60] whereas the rotational constants of D_2 and HD are 1/2 and 3/4 that of H_2, respectively. Because isotopic substitution involves a much larger change in B_{rot} than in polarizability, $|\Delta B^{2nd\ EQQ}|\gg|\Delta B^{Ind}|$. Also, because of the $-\Gamma^2/B_{rot}$ dependence of second order EQQ and the μ^{-1} dependence of B_{rot},[50] $\Delta B^{2nd\ EQQ}$ is negative and its magnitude is larger for an o-H_2/o-D_2 pair relative to the analogous o-H_2/HD pair. The increase in $|\Delta B^{2nd\ EQQ}|$ upon impurity vibrational excitation is due to an increase in Γ[16,63] and decrease in B_{rot}.[50]

Kokshenev used a different approach to calculate ΔB for nn o-H_2/o-D_2 and o-H_2/HD pairs[39] and obtained much larger values than did Byers and Oka. In this approach, an *isotope-independent* anisotropic potential $B(R)$ was used to describe $J=1/J=0$ pairwise anisotropic interactions. Similar to the potential shown in Fig. 9(b), Kokshenev's potential contained a repulsive valence term which fell off exponentially with increasing R and an attractive dispersion term with R^{-6} dependence. $\langle\Delta B\rangle$ was calculated from the difference in $\langle\Psi(R)|B(R)|\Psi(R)\rangle$ for a o-H_2/o-D_2 or o-H_2/HD nn impurity pair relative to the analogous unsubstituted o-H_2/p-H_2 pair. The nonzero ΔB resulted from the difference in the intermolecular wave function $\Psi(R)$ of the impurity pair relative to that of the unsubstituted pair. That is, Kokshenev computed the changes in *renormalization* which accompany isotopic substitution. Renormalization is particularly important in the solid parahydrogen crystal because the zero-point lattice motion of molecules is an appreciable fraction of R_0. For H_2 molecules, the rms width of a single molecule distribution function[64] is ~0.18 R_0 and this width should have a strong mass dependence.

There are two interesting results from Kokshenev's work. First, for an o-H_2/p-H_2 nn pair, $\langle B\rangle$ is actually *repulsive*, with a value of $\sim+7$ cm^{-1}. Also, $\langle\Delta B\rangle$ is calculated to be ~-1.4 and ~-1 cm^{-1} for o-H_2/o-D_2 and o-H_2/HD nn impurity pairs, respectively. Both results can be qualitatively understood from the potential curves shown in Fig. 9. In these curves, the minimum of the anisotropic pair potential (~4.2 Å)[5,56] is greater than both R_e of the isotropic potential (~3.3 Å)[5,55] and R_0 (~3.78 Å).[2] Since the isotropic intermolecular potential dominates at most R, $\Psi(R)$ reflects its properties and has appreciable amplitude at the repulsive inner wall of $B(R)$. Hence, $\langle B\rangle$ is positive. Because of the heavier mass of the isotopic impurity, $\Psi(R)_{imp.pair}$ has less amplitude at the R extrema than does $\Psi(R)_{o\text{-}H_2/p\text{-}H_2}$. Consequently, $\langle B\rangle_{imp.pair}$ has a smaller contribution from the repulsive part of the potential than does $\langle B\rangle_{o\text{-}H_2/p\text{-}H_2}$. As $\langle\Delta B\rangle = \langle B\rangle_{imp.pair} - \langle B\rangle_{o\text{-}H_2/p\text{-}H_2}$, $\langle\Delta B\rangle$ is negative and $|\langle\Delta B_{D_2}\rangle| > |\langle\Delta B_{HD}\rangle|$. In Kokshenev's model, $\langle B\rangle$ and $\langle\Delta B\rangle$ depended only on the masses of the pair molecules and not on the vibrational state of the $J=0$ isotopic impurity.

Both Byers and Oka and Kokshenev predict a negative sign for ΔB, in agreement with experiment. In addition, both theoretical approaches predict that $|\Delta B_{D_2}| > |\Delta B_{HD}|$, also in accord with experiment. Finally, Byers and Oka's calculations predict an increase in $|\Delta B|$ upon vibrational excitation, as was observed experimentally. Quantitatively, however, the calculations of Byers and Oka underestimate $|\Delta B|$ by about an order of magnitude while those of Kokshenev overestimate $|\Delta B|$ by about a factor of 5. The two computational approaches are quite complementary in that Byers and Oka calculated specific *isotope-dependent* interactions of $J=1/J=0$ pairs in a lattice with a fixed *isotope-independent* nn distance R_0, while Kokshenev averaged an *isotope-independent* $J=1/J=0$ anisotropic potential over the *isotope-dependent* nn intermolecular wave functions $\Psi(R)$.

As a final note, we consider a connection between the experimental ΔB_{vib} values [cf. Eq. (13)] and Kokshenev's calculation of $\langle B \rangle$. Using Eqs. (6) and (13), as well as the approximation that induction and dispersion make the largest contributions to ΔB_{vib}, we derive an expression

$$\langle B^{v=0}_{ind./disp.} \rangle = \left(\frac{\alpha_{v=0}}{\alpha_{v=0} - \alpha_{v=1}} \right) \Delta B_{vib}, \tag{14}$$

where v and α refer respectively to the vibrational quantum number and isotropic polarizability of the isotopic impurity. Inserting the experimental ΔB_{vib} values and known polarizabilities[60] into Eq. (14), we calculate that $\langle B_{ind/disp} \rangle$ is -2.9 cm^{-1} for o-$H_2/v=0$ o-D_2 or o-$H_2/v=0$ HD nn impurity pairs. This experimentally derived $\langle B_{ind/disp} \rangle$ agrees to within 0.2 cm^{-1} of $\langle B_{disp} \rangle$ calculated from Kokshenev's renormalization approach. This quantitative agreement suggests: (1) the polarizability vibrational dependence of dispersion makes the principal contribution to ΔB_{vib}; and (2) Kokshenev accurately computed $\langle B_{disp} \rangle$ of nn impurity pairs. The main quantitative problem in his ΔB calculations probably lies in renormalization of valence interactions.

2. Nearest-neighbor ΔB_{diff} parameter

We now consider the small ip/oop differences in ΔB for the same type of nn pair. In previous work, a difference in ip/oop parameters had been found in fitting the EQQ parameter Γ to the microwave spectra of nn o-H_2 pairs.[7] In our case, we define the parameter

$$\Delta B_{diff} = |\Delta B_{oop}| - |\Delta B_{ip}|, \tag{15}$$

which varies from $+0.0227$ cm^{-1} for the o-$H_2/v=0$ o-D_2 nn pair to -0.008 cm^{-1} for the o-$H_2/v=1$ HD nn pair (cf. Table V). We qualitatively explain the variation of ΔB_{diff} with pair type through the effects of local lattice distortion by the isotopic impurity, where this distortion is slightly different for the ip and oop nn of the impurity.[65]

Extending the ideas of Kokshenev[39] (cf. Sec. VI B 1) we argue that $\langle B \rangle_{imp.pair}$ depends on the intermolecular wave function $\Psi(R)_{imp.pair}$, which in turn depends on the amount of local lattice distortion. It follows that with different amounts of ip/oop lattice distortion, $\Delta B_{ip} \neq \Delta B_{oop}$, even for an impurity pair with the same $J=0$ isotope in the same vibrational state. We make the simplifying assumption that *differential* ip/oop distortion scales with the *total* distortion, so that ΔB_{diff} also scales with the *total* distortion.

To understand local lattice distortion by D_2 and HD isotopic impurities, we turn to previous experimental work as well as to our physical intuition. Analysis of microwave spectra[10] has determined a 0.34% local reduction in R_0 around a $v=0$ o-D_2 impurity in a parahydrogen lattice. Because of its smaller zero-point motion, the heavier isotopic impurity draws in the neighboring H_2 molecules. This sort of lattice contraction was already discussed in Sec. VI A 1 as an explanation for the observed red shift of the nn p-D_2/o-D_2 $Q_1(0)$ features. In the present context, we propose that the heavier D_2 impurity causes greater lattice contraction than the lighter HD impurity.[66] For both D_2 and HD, we also propose that vibrational excitation tends to counteract the impurity induced contraction. These proposals are supported by earlier work on the related systems of D_2/rare gas and H_2/rare gas dimers.[67] Experimentally derived potentials reveal that the intermolecular R_0 of a particular D_2/rare gas dimer is slightly shorter than the R_0 of the analogous H_2/rare gas dimer, and also that these R_0 increase upon excitation of either the D_2 or H_2 stretching vibration. We rely on this analysis rather than on interpretation of fitted rotational constants of dimers containing H_2 and/or D_2.[68,69]

Experimentally, the variation of ΔB_{diff} with impurity pair type matches the expected changes in total local (and hence differential ip/oop) contraction. ΔB_{diff} is greater for nn o-$H_2/v=0$ o-D_2 than for nn o-$H_2/v=0$ HD and decreases for both types of pairs upon vibrational excitation. For the impurity pair containing $v=1$ HD, $\Delta B_{diff} \sim 0$, indicating little local lattice distortion. This lattice distortion model also explains the variation of ϵ_{2c} with impurity pair type (cf. Sec. VI B 4).

3. Next-nearest-neighbor ΔB parameter

ΔB_{nnn} was only determined for o-H_2/HD nnn pairs (cf. Table V). Like ΔB_{nn}, ΔB_{nnn} has a negative sign and its magnitude increases upon HD vibrational excitation. For the o-H_2/HD pair, $|\Delta B_{nnn}|$ is an order of magnitude smaller than $|\Delta B_{nn}|$, which matches the eightfold decrease in attractive dispersion interactions derived from $(R_{nnn}/R_{nn})^{-6}$ and $R_{nnn} = \sqrt{2} R_{nn}$.

4. ϵ_{2c} parameter

Our final discussion topic concerns the anisotropic crystal field parameter ϵ_{2c}, which represents the anisotropic interactions of an impurity $J=1$ molecule with a lattice of p-H_2 molecules [cf. Eq. (4)]. We initially focus on nn impurity pairs. As listed in Table V, the experimental values of nn ϵ_{2c} vary from -0.0160 to $+0.0400$ cm^{-1}, depending on the particular $J=0$ isotope, its vibrational state, and also on the ip/oop geometric configuration of the pair. These $|\epsilon_{2c}|$ are 5 to 40 times smaller than their respective $|\Delta B|$ and are the same order of magnitude as the ϵ_{2c} of isolated o-H_2, -0.0118 cm^{-1}.[18] The impurity pair ϵ_{2c} are largely derived from $|11_+\rangle/|11_-\rangle$ splittings (cf. Table III). The estimated

measurement error of these splittings is only ± 0.001 cm^{-1}, so the wide variation in impurity pair ϵ_{2c} must have some physical meaning.

In Eq. (4), ϵ_{2c} is derived from the sum of all pairwise anisotropic interactions of an isolated $J=1$ impurity in a hcp parahydrogen lattice. With a single $R_{nn}=R_0$, this sum vanishes for the nn and nnn shells of p-H_2 molecules[57] and is independent of impurity pair type. Hence, ϵ_{2c} should be both small and *single valued* in a perfect hcp lattice. At this level, the impurity pair model does not explain the wide variation of ϵ_{2c}. However, the isotopic impurity can impact ϵ_{2c} through *local* lattice distortion, disrupting the pure hcp crystal symmetry about the $J=1$ impurity and changing the individual $\langle B_{H_2}\rangle_i$ in the ϵ_{2c} lattice sum. Because lattice distortion varies with the mass, vibrational state, and the ip/oop configuration of the $J=0$ isotopic impurity, ϵ_{2c} will also depend on these factors. To further clarify the observed ϵ_{2c} variation, we calculate a *difference* ϵ_{2c} parameter

$$\Delta\epsilon_{2c}=\epsilon_{2c}^{ic}-\epsilon_{2c}^{pc}, \tag{16}$$

where ϵ_{2c}^{ic} and ϵ_{2c}^{pc} are experimental impurity crystal field and pure crystal field parameters, respectively. Table V lists $\Delta\epsilon_{2c}$ values.

To explain the $\Delta\epsilon_{2c}$, we use the same qualitative picture of lattice contraction that was presented in the ΔB_{diff} discussion (cf. Sec. VI B 2). We note, that the ϵ_{2c} lattice sum is centered around the $J=1$ *impurity* while lattice distortion is centered around the *isotopic impurity*. In the ϵ_{2c} sum, the largest contributions are from the nn and nnn of the $J=1$ impurity, while lattice distortion is strongest for the nn of the isotopic impurity. The isotopic and $J=1$ impurities share four mutual nn (cf. Fig. 10), and for a small isotropic contraction of the nn of the isotopic impurity, R_i is slightly smaller than R_0 for five nn in the ϵ_{2c} lattice sum (counting the isotopic impurity site). For an ip impurity pair, three of these distorted nn will be ip and two will be oop, and for an oop impurity pair, two will be ip and three will be oop. There are also two distorted nnn in the ϵ_{2c} lattice sum, but they contribute negligibly to ϵ_{2c}, as will be shown below.

In evaluating ϵ_{2c}, we only consider the effects of small changes in R_i on the $m=0$ term of the lattice sum of Eqs. (4) and (5). Our approximations are: (1), the Ω_i are not changed by the lattice distortion; and (2), there is still nearly complete hcp cancellation of the $m\neq 0$ terms in the sum. We are only considering the largest effect of a small isotropic lattice contraction.

In the ϵ_{2c} lattice sum, the values of $C_{20}(\Omega_i)$ for Ω_{ip}, Ω_{oop}, and Ω_{nnn} are $-1/2$, $+1/2$, and 0, respectively. Hence, we can ignore the nnn and only consider the nn sum $\Sigma\, B_{H_2}(R_i)C_{20}(\Omega_i)$. This sum vanishes for the undistorted lattice because the six ip and six oop nn have contributions of equal magnitude and opposite sign. In the distorted impurity crystal lattice, the $J=1$ impurity has seven undistorted nn and five distorted nn, with different pairwise contributions to ϵ_{2c}, $\langle B_{undis}\rangle$ and $\langle B_{dis}\rangle$, respectively. In his renormalization calculations, Kokshenev estimated $\langle B_{undis}\rangle$ to be $\sim +7$ cm^{-1}, where the positive sign is a due to the large contribution from the repulsive inner wall of the anisotropic potential. With lattice contraction, we would expect an even greater contribution from this repulsive wall, and the inequality $\langle B_{dis}\rangle > \langle B_{undis}\rangle$. After considering the different numbers of distorted ip and oop nn molecules, the unequal values of $\langle B_{undis}\rangle$ and $\langle B_{dis}\rangle$, and the unequal values of $C_{20}(\Omega_{ip})$ and $C_{20}(\Omega_{oop})$, the net impurity crystal contribution to the nn ϵ_{2c} lattice sum is

$$\Delta\epsilon_{2c}^{ip}=1/2(\langle B_{undis}\rangle-\langle B_{dis}\rangle) \tag{17a}$$

and

$$\Delta\epsilon_{2c}^{oop}=1/2(\langle B_{dis}\rangle-\langle B_{undis}\rangle), \tag{17b}$$

for ip and oop impurity pairs, respectively. With this sign difference between $\Delta\epsilon_{2c}^{ip}$ and $\Delta\epsilon_{2c}^{oop}$, as well as the predicted dependence of $\langle B_{dis}\rangle$ on lattice contraction, we are able to explain the wide variation of ϵ_{2c} values with impurity pair type (cf. Table V).

We illustrate with the o-$H_2/v=0$ o-D_2 nn pair. Physical arguments predict that of all the isotopic impurities studied, $v=0$ o-D_2 should cause the greatest local lattice contraction and hence the most positive value of $\langle B_{dis}\rangle-\langle B_{undis}\rangle$. Inserting a positive value of $\langle B_{dis}\rangle-\langle B_{undis}\rangle$ into Eq. (17) gives a negative $\Delta\epsilon_{2c}^{ip}$ and a positive $\Delta\epsilon_{2c}^{oop}$, consistent with the signs of the experimental $\Delta\epsilon_{2c}^{ip}$ and $\Delta\epsilon_{2c}^{oop}$. Additionally, the experimental $|\Delta\epsilon_{2c}^{ip(oop)}|$ is largest for ip (oop) o-$H_2/v=0$ o-D_2 pairs relative to those of any other ip (oop) pair type, consistent with the biggest lattice contraction around $v=0$ o-D_2. Finally, $|\Delta\epsilon_{2c}^{ip}| \neq |\Delta\epsilon_{2c}^{oop}|$, indicating ip/oop differences in $\langle B_{dis}\rangle$. Like the nonzero values of ΔB_{diff} (cf. Sec. VI B 2), the ip/oop differences for $\langle B_{dis}\rangle$ support the notion of different amounts of lattice contraction for ip and oop nn of the isotopic impurity. Unfortunately, the three anisotropic potential terms $\langle B_{undis}\rangle$, $\langle B_{dis}^{ip}\rangle$, and $\langle B_{dis}^{oop}\rangle$ cannot be quantitatively derived from only two experimental parameters, $\Delta\epsilon_{2c}^{ip}$ and $\Delta\epsilon_{2c}^{oop}$, of any given pair type.

The experimental inequalities $\Delta\epsilon_{2c}^{oop}>0>\Delta\epsilon_{2c}^{ip}$ also hold for the o-$H_2/v=0$ HD nn impurity pair, but the $|\Delta\epsilon_{2c}^{ip(oop)}|$ are smaller than the respective $|\Delta\epsilon_{2c}^{ip(oop)}|$ of the o-$H_2/v=0$ o-D_2 nn impurity pair. These data indicate that the lattice contracts around $v=0$ HD and that this contraction is less than around $v=0$ o-D_2. The smaller values of $|\Delta\epsilon_{2c}|$ for o-$H_2/v=1$ o-D_2 nn impurity pairs relative to o-$H_2/v=0$ o-D_2 nn impurity pairs indicate that vibrational excitation reduces $\langle B_{dis}\rangle$, probably because of less lattice contraction. For o-$H_2/v=1$ HD nn impurity pairs, $\Delta\epsilon_{2c}^{ip}$, $\Delta\epsilon_{2c}^{oop}\sim 0$, indicating little lattice distortion by the $v=1$ HD impurity. This is all consistent with ΔB_{diff} analysis of Sec. VI B 2.

VII. SUMMARY AND CONCLUSIONS

This work is the first comprehensive observation and analysis of the high-resolution infrared $Q_1(0)$ spectra of impurity D_2 and HD in solid parahydrogen. Each impurity has a spectrum composed of $\sim$100 sharp lines spread over $\sim$0.4 cm^{-1}. The linewidths vary, but are of order of magnitude 10 MHz. These spectra make clear: (1) the infrared $Q_1(0)$ transitions of $J=0$ isotopic impurities are induced by the qua-

drupolar fields of nearby impurity $J=1$ molecules; and (2) the spectral pattern of strong $Q_1(0)$ lines is due to the splitting of the M-orientational levels of nn $J=1/J=0$ o-D_2 or nn $J=1/J=0$ HD impurity pairs. Using the theories of Sears and Van Kranendonk,[36] Kokshenev,[39] and Byers and Oka,[24,51] the strong lines in the D_2 and HD spectra can be individually and unambiguously assigned as specific quantum state $Q_1(0)$ transitions of nn impurity pairs containing p-D_2/o-D_2 or o-H_2/o-D_2, and o-H_2/HD, respectively. The assigned transitions of nn pairs containing o-H_2 are confirmed by combination differences which agree to at least 5×10^{-4} cm^{-1}, the instrumental precision. These assignments yield complete $Q_1(0)$ energy level diagrams for nn impurity pair o-H_2/o-D_2 and o-H_2/HD embedded in solid parahydrogen. The remaining unassigned transitions in both the D_2 and HD spectra are weak. In both the D_2 (HD) spectra, there is a cluster of lines around the isolated D_2 (HD) $Q_1(0)$ transition frequency which we ascribe to $Q_1(0)$ transitions of more distant neighbor o-H_2/o-D_2 (o-H_2/HD) impurity pairs. We have specifically assigned some of these lines as nnn impurity pair transitions. The remaining weak features in both spectra are likely due to impurity triples and larger clusters which contain various mixtures of $J=1$ and isotopic impurities. In comparing the D_2 and HD $Q_1(0)$ spectra, we observe a striking pattern similarity of these weaker features.

We find that the average $Q_1(0)$ frequency of nn o-H_2/o-D_2 impurity pairs approximately equals the $Q_1(0)$ transition frequency of isolated o-D_2 molecules. The small ($\sim$0.008 cm^{-1}) average red shift of the pair transitions is ascribed to the increased isotropic intermolecular interactions of a $J=1/J=0$ pair relative to those of a $J=0/J=0$ pair. There is also a larger 0.03 cm^{-1} red shift of the nn p-D_2/o-D_2 $Q_1(0)$ features relative to their o-H_2/o-D_2 counterparts. We attribute this shift to the increased isotropic interactions resulting from lattice contraction around the heavier D_2 impurities.

Our analysis also shows that the M-orientational splittings of the $J=1/J=0$ nn impurity pair energies depend strongly on the particular $J=0$ isotope, its vibrational state, and also on the pair geometric configuration (ip vs oop). These splittings can be fit to an impurity pair model with two anisotropic potential parameters, ΔB and ϵ_{2c}. These parameters describe the anisotropic interactions of a single $J=1$ molecule with the surrounding $J=0$ lattice. The ΔB parameter contains most of the contributions resulting from replacement of a $J=0$ p-H_2 molecule with a $J=0$ isotopic impurity. The experimental values of ΔB_{nn} vary from -0.1 to -0.4 cm^{-1}, with larger $|\Delta B|$ for $J=0$ D_2 than for $J=0$ HD. $|\Delta B|$ also increases upon vibrational excitation of the $J=0$ isotopic impurity and this increase is quantitatively consistent with the $\mu^{-1/2}$ v vibrational dependence of the hydrogenic molecular constants. The ΔB values appear to reflect the significant changes in renormalization due to the greater mass of the isotopic impurity.

The other parameter in the impurity pair model is ϵ_{2c}, which represents the anisotropic interactions of an isolated impurity $J=1$ molecule with a lattice of p-H_2 molecules. The analysis of spectral splittings yields $|\epsilon_{2c}|$ values which, depending on the pair type, are 5 to 40 times smaller than the respective $|\Delta B|$ values. Our values of $|\epsilon_{2c}|$ qualitatively agree with previous experimental and theoretical work. However, ϵ_{2c} should be single valued in a perfect hcp lattice and our ϵ_{2c} values vary widely in both sign and magnitude. Like the analogous impurity pair ΔB values, these experimental ϵ_{2c} values depend on the particular $J=0$ isotope, its vibrational state, and also on the geometric ip/oop configuration of the nn impurity pair. We are able to qualitatively explain much of the variation in ΔB and ϵ_{2c} through the effects of lattice distortion by the isotopic impurity.

This paper summarizes a fairly comprehensive study of impurity isotope $Q_1(0)$ spectroscopy. However, there is still a need for further experimental and theoretical work on this system. Experimentally, it would be interesting to complete the observation of the nn p-D_2/o-D_2 $Q_1(0)$ features, as well as to observe the analogous nn p-D_2/HD spectra. These direct infrared spectra, along with the analogous Stark field (isolated impurity) spectra, would give a complete set of data on the impurity isotope $Q_1(0)$ system. These data should confirm or dispute the lattice distortion explanations put forth in this paper. The complete set of experimental ΔB and ϵ_{2c} values would also provide a guide to theoretical efforts at modeling the anisotropic interactions of these impurity pair systems. An important goal of these efforts is a deeper and more quantitative understanding of the quantum crystal nature of solid parahydrogen.

In addition, we would also like to understand better the numerous weaker features in the present spectra. In particular, we have not yet made a concentrated effort to assign them as specific transitions of particular impurity triples or larger clusters.[70,71] The distinctive spectral pattern and polarization dependences of these features should be a useful guide to unraveling their complexity.

We conclude by emphasizing one of the achievements of the present work. This work is not only one of the few cases in which high-resolution laser spectroscopy has been successfully applied to a condensed phase system, but it is also one of the much smaller subset of these cases in which many of the transitions have rigorous quantum state assignments. These assignments yield complete energy level diagrams which semiquantitatively fit a physically reasonable impurity pair model. Although this sort of assignment, analysis and understanding is ubiquitous in high-resolution gas phase spectroscopy, it has rarely been achieved in high-resolution condensed phase spectroscopy. In the specific system of solid parahydrogen, many of the high-resolution spectra have not yet been clearly assigned and understood, but we hope that the present studies will provide some insight into these more complex spectra.

ACKNOWLEDGMENTS

We would like to thank Dr. Robert Curl for lending us the CdTe modulator used in this work. We also thank Dr. Mary-Frances Jagod for the software used for data acquisition and measurement. We thank Robert Dickson for a critical reading of this paper. This work was supported by the

United States Air Force. D.P.W. acknowledges an AT&T Ph.D. scholarship, K.E.K. acknowledges an NSF graduate fellowship and T. M. acknowledges an overseas scholarship from the Ministry of Education, Science, and Culture of Japan.

[1] A. H. Francis and R. Kopelman, in *Topics in Applied Physics: Laser Spectroscopy of Solids*, edited by W. M. Yen and P. M. Selzer (Springer, Berlin, 1986), pp. 241–305. For a collection of articles on solid state relaxation, see Chem. Phys. **128**, No. 1 (1988).
[2] P. C. Souers, *Hydrogen Properties for Fusion Energy* (University of California, Berkeley, 1986).
[3] E. J. Allin, W. F. J. Hare, and R. E. MacDonald, Phys. Rev. **98**, 554 (1955).
[4] J. Van Kranendonk and G. Karl, Rev. Mod. Phys. **40**, 531 (1968), and references therein.
[5] J. Van Kranendonk, *Solid Hydrogen* (Plenum, New York, 1983).
[6] W. N. Hardy and A. J. Berlinsky, Phys. Rev. Lett. **34**, 1520 (1975).
[7] W. N. Hardy, A. J. Berlinsky, and A. B. Harris, Can. J. Phys. **55**, 1150 (1977).
[8] A. B. Harris, A. J. Berlinsky, and W. N. Hardy, Can. J. Phys. **55**, 1180 (1977).
[9] B. W. Statt, W. N. Hardy, and R. Jochemsen, Can. J. Phys. **58**, 1326 (1980).
[10] B. W. Statt and W. N. Hardy, Can. J. Phys. **58**, 1341 (1980).
[11] R. Jochemsen, B. W. Statt, and W. N. Hardy, Can. J. Phys. **58**, 1356 (1980).
[12] T. Oka, Annu. Rev. Phys. Chem. **44**, 299 (1993).
[13] D. P. Weliky, T. J. Byers, K. E. Kerr, T. Momose, R. M. Dickson, and T. Oka, Appl. Phys. B **59**, 265 (1994).
[14] M.-C. Chan, M. Okumura, C. M. Gabrys, L.-W. Xu, B. D. Rehfuss, and T. Oka, Phys. Rev. Lett. **66**, 2060 (1991).
[15] T. Momose, D. P. Weliky, and T. Oka, J. Mol. Spectrosc. **153**, 760 (1992).
[16] R. A. Steinhoff, K. V. S. R. Apparao, D. W. Ferguson, K. N. Rao, B. P. Winnewisser, and M. Winnewisser, Can. J. Phys. **72**, 1122 (1994).
[17] R. M. Dickson, T. Momose, T. J. Byers, and T. Oka Phys. Rev. B (submitted).
[18] R. M. Dickson, T. J. Byers, and T. Oka, J. Low Temp. Phys. **102**, 241 (1996).
[19] Y. Zhang, T. J. Byers, D. P. Weliky, and T. Oka (in preparation).
[20] E. Goovaerts, X. Y. Chen, A. Bouwen, and D. Schoemaker, Phys. Rev. Lett. **57**, 479 (1986).
[21] M.-C. Chan, S. S. Lee, M. Okumura, and T. Oka, J. Chem. Phys. **95**, 88 (1991).
[22] M. Okumura, M.-C. Chan, and T. Oka, Phys. Rev. Lett. **62**, 32 (1989).
[23] K. E. Kerr, T. J. Byers, B. F. Ventrudo, T. Momose, D. T. Cassidy, and T. Oka, Forty-seventh Symposium on Molecular Spectroscopy, The Ohio State University, 1992, paper RG03.
[24] T. J. Byers, Ph.D. thesis, University of Chicago, 1995.
[25] R. A. Steinhoff, B. P. Winnewisser, and M. Winnewisser, Phys. Rev. Lett. **73**, 2833 (1994).
[26] K. E. Kerr, T. Momose, D. P. Weliky, C. M. Gabrys, and T. Oka, Phys. Rev. Lett. **72**, 3957 (1994).
[27] M.-C. Chan, L.-W. Xu, C. M. Gabrys, and T. Oka, J. Chem. Phys. **95**, 9404 (1991).
[28] A. R. W. McKellar and M. J. Clouter, Can. J. Phys. **68**, 422 (1990).
[29] M.-C. Chan, S. Lee, and T. Oka, Forty-fourth Symposium on Molecular Spectroscopy, The Ohio State University, 1989, paper TG3.
[30] M.-C. Chan, Ph.D. thesis, University of Chicago, 1991.
[31] M.-C. Chan, S. S. Lee, and T. Oka (unpublished).
[32] H. P. Gush, W. F. J. Hare, E. J. Allin, and H. L. Welsh, Can. J. Phys. **38**, 176 (1960).
[33] S. S. Bhatnagar, E. J. Allin, and H. L. Welsh, Can. J. Phys. **40**, 9 (1962).
[34] M. Okumura, M.-C. Chan, B. D. Rehfuss, and T. Oka (unpublished).
[35] D. P. Weliky, K. E. Kerr, and T. Oka (in preparation).
[36] V. F. Sears and J. Van Kranendonk, Can. J. Phys. **42**, 980 (1964).
[37] M. Leblans, A. Bouwen, C. Sierens, W. Joosen, E. Goovaerts, and D. Schoemaker, Phys. Rev. B **40**, 6674 (1989).
[38] V. G. Manzhelii, V. A. Popov, G. P. Chausov, and L. I. Vladimirova, J. Low Temp. Phys. **14**, 397 (1974).
[39] V. B. Kokshenev, Sov. J. Low Temp. Phys. **2**, 118 (1976).
[40] E. J. Allin, T. Feldman, and H. L. Welsh, J. Chem. Phys. **24**, 1116 (1956).
[41] M. F. Crawford and I. R. Dagg, Phys. Rev. **91**, 1569 (1953).
[42] L. H. Nosanow, Phys. Rev. **146**, 120 (1966).
[43] H. M. Pickett, Appl. Opt. **19**, 2745 (1980).
[44] C. S. Gudeman, M. H. Begemann, J. Pfaff, and R. J. Saykally, Opt. Lett. **8**, 310 (1983).
[45] H. Adams, J. L. Hall, R. F. Curl, J. V. V. Kasper, and F. K. Tittel, J. Opt. Soc. Am. B **1**, 710 (1984).
[46] M.-C. Chan, J. Mol. Spectrosc. **153**, 750 (1992).
[47] D. P. Weliky, Ph.D. thesis, University of Chicago, 1995.
[48] K. E. Kerr, D. P. Weliky, T. Momose, R. M. Dickson, and T. Oka, Forty-ninth Symposium on Molecular Spectroscopy, The Ohio State University, 1994, paper MF02.
[49] K. E. Kerr, Ph.D. thesis, University of Chicago, 1995.
[50] K. P. Huber and G. Herzberg, *Molecular Spectra and Molecular Structure, Vol. IV, Constants of Diatomic Molecules* (Van Nostrand Reinhold, New York, 1979), pp. 258–259, 266–267.
[51] T. J. Byers and T. Oka (in preparation).
[52] T. Nakamura, Prog. Theor. Phys. Kyoto **14**, 135 (1955).
[53] W. N. Hardy and J. R. Gaines, Phys. Rev. Lett. **19**, 1417 (1967).
[54] R. Schweizer, S. Washburn, and H. Meyer, J. Low Temp. Phys. **37**, 289 (1979).
[55] I. F. Silvera and V. V. Goldman, J. Chem. Phys. **69**, 4209 (1978).
[56] G. A. Gallup, Mol. Phys. **33**, 943 (1977).
[57] This is easily derived from the known angles of the hcp parahydrogen lattice (Ref. 5). For the 12 nn, the values of θ are: $\cos^{-1}(0)$ for 6 ip, $\cos^{-1}(\sqrt{2/3})$ for 3 oop, and $\cos^{-1}(-\sqrt{2/3})$ for 3 oop. For the second shell of 6 nnn, the values of θ are: $\cos^{-1}(\sqrt{1/3})$ for 3 and $\cos^{-1}(-\sqrt{1/3})$ for 3.
[58] D. P. Weliky, K. E. Kerr, T. J. Byers, Y. Zhang, T. Momose, and T. Oka (in preparation).
[59] M. Trefler and H. P. Gush, Phys. Rev. Lett. **20**, 703 (1968).
[60] W. Kolos and L. Wolniewicz, J. Chem. Phys. **46**, 1426 (1967).
[61] A. Birnbaum and J. D. Poll, J. Atmos. Sci. **26**, 943 (1969).
[62] J. D. Poll and L. Wolniewciz, J. Chem. Phys. **68**, 3053 (1978).
[63] T. K. Balasubramanian, C.-H. Lien, J. R. Gaines, K. N. Rao, and E. K. Damon, J. Mol. Spectrosc. **92**, 77 (1982).
[64] I. F. Silvera, Rev. Mod. Phys. **52**, 393 (1980).
[65] Differential lattice distortion has previously been considered in the analysis of the crystal field parameter ϵ_{2c}. J. C. Raich and L. B. Kanney, J. Low Temp. Phys. **28**, 95 (1977) show that this distortion should lead to a negative ϵ_{2c}; see also S. Luryi and J. Van Kranendonk, Can. J. Phys. **57**, 933 (1979).
[66] The contraction around a heteronuclear HD impurity should also be smaller because unlike D_2, HD rotates slightly off its center-of-mass and has a larger effective volume than D_2 (Ref. 10).
[67] R. J. Le Roy and J. M. Hutson, J. Chem. Phys. **86**, 837 (1987).
[68] A. R. W. McKellar, Faraday Discuss. Chem. Soc. **73**, 89 (1982).
[69] A. R. W. McKellar, J. Chem. Phys. **92**, 3261 (1990).
[70] H. Miyagi, Prog. Theor. Phys. **40**, 1448 (1968).
[71] A. Mishima and H. Miyagi, J. Phys. Soc. Jpn. **56**, 1815 (1987).